

OpenViewer: Openness-Aware Multi-View Learning

Shide Du^{1,2}, Zihan Fang^{1,2}, Yanchao Tan^{1,2}, Changwei Wang³, Shiping Wang^{1,2}, Wenzhong Guo^{1,2*}

¹ College of Computer and Data Science, Fuzhou University, Fuzhou, China

² Fujian Provincial Key Laboratory of Network Computing and Intelligent Information Processing, Fuzhou University, Fuzhou, China

³ Key Laboratory of Computing Power Network and Information Security, Ministry of Education, Shandong Computer Science Center, Qilu University of Technology, Jinan, China

dushidems@gmail.com, fzihan11@163.com, yctan@fzu.edu.cn, changweiwang@sdas.org, shipingwangphd@163.com, guowenzhong@fzu.edu.cn

Abstract

Multi-view learning methods leverage multiple data sources to enhance perception by mining correlations across views, typically relying on predefined categories. However, deploying these models in real-world scenarios presents two primary openness challenges. **1) Lack of Interpretability:** The integration mechanisms of multi-view data in existing black-box models remain poorly explained; **2) Insufficient Generalization:** Most models are not adapted to multi-view scenarios involving unknown categories. To address these challenges, we propose OpenViewer, an openness-aware multi-view learning framework with theoretical support. This framework begins with a Pseudo-Unknown Sample Generation Mechanism to efficiently simulate open multi-view environments and previously adapt to potential unknown samples. Subsequently, we introduce an Expression-Enhanced Deep Unfolding Network to intuitively promote interpretability by systematically constructing functional prior-mapping modules and effectively providing a more transparent integration mechanism for multi-view data. Additionally, we establish a Perception-Augmented Open-Set Training Regime to significantly enhance generalization by precisely boosting confidences for known categories and carefully suppressing inappropriate confidences for unknown ones. Experimental results demonstrate that OpenViewer effectively addresses openness challenges while ensuring recognition performance for both known and unknown samples.

Introduction

Multi-view learning has emerged as a prominent area of artificial intelligence, focusing on leveraging diverse data sources to enhance perception (Tan et al. 2024; Yu et al. 2024b). This learning paradigm processes real-world objects from various extractors or sensors, exploiting correlations across multiple views to enhance performance in applications like computer vision (Ning et al. 2024), natural language processing (Song et al. 2024), large-scale language models (Guo et al. 2023), and more (Pei et al. 2023; Ye and Li 2024). However, traditional multi-view methods, whether heuristic (Zhang et al. 2023; Xiao et al. 2024) or deep learning (Xu et al. 2023; Yang et al. 2024), typically

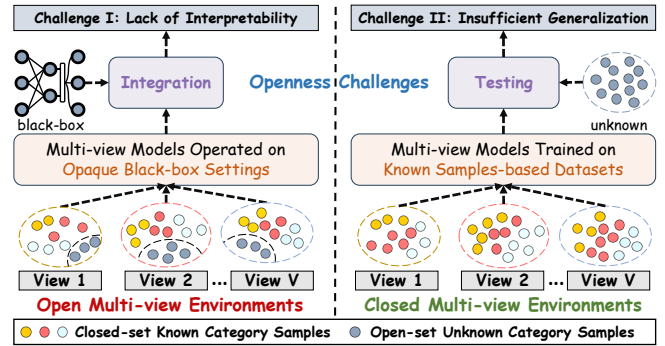


Figure 1: Two multi-view environments and challenges.

operate under the assumption that all samples belong to known categories (Du et al. 2023). When deployed in real-world settings, these approaches encounter two significant openness challenges, as illustrated in Fig. 1. **Challenge I: Lack of Interpretability.** These black-box methods often lack of explanation in the integration process of multi-view data involving both known and unknown category samples. This opacity undermines their reliability in open scenarios. **Challenge II: Insufficient Generalization.** Trained on known samples-based datasets, existing multi-view closed-set methods fail to identify unknown categories during testing, frequently mislabeling them as known with unduly high confidences. Consequently, they struggle to generalize to multi-view environments containing unknown samples. This issue arises because the models are not preemptively adapted to the range of potential unknown categories.

To effectively address these challenges, we propose OpenViewer, an openness-aware multi-view learning framework designed for real-world environments, as outlined in Fig. 2. OpenViewer starts with a pseudo-unknown sample generation mechanism, allowing the model to efficiently simulate open multi-view environments and previously adapt to potential unknown samples. Grounded on ADMM iterative solutions with functionalized priors, we derive an interpretable multi-view feature expression-enhanced deep unfolding network, comprising redundancy removal, dictionary learning, noise processing, and complementarity fu-

*Corresponding author.

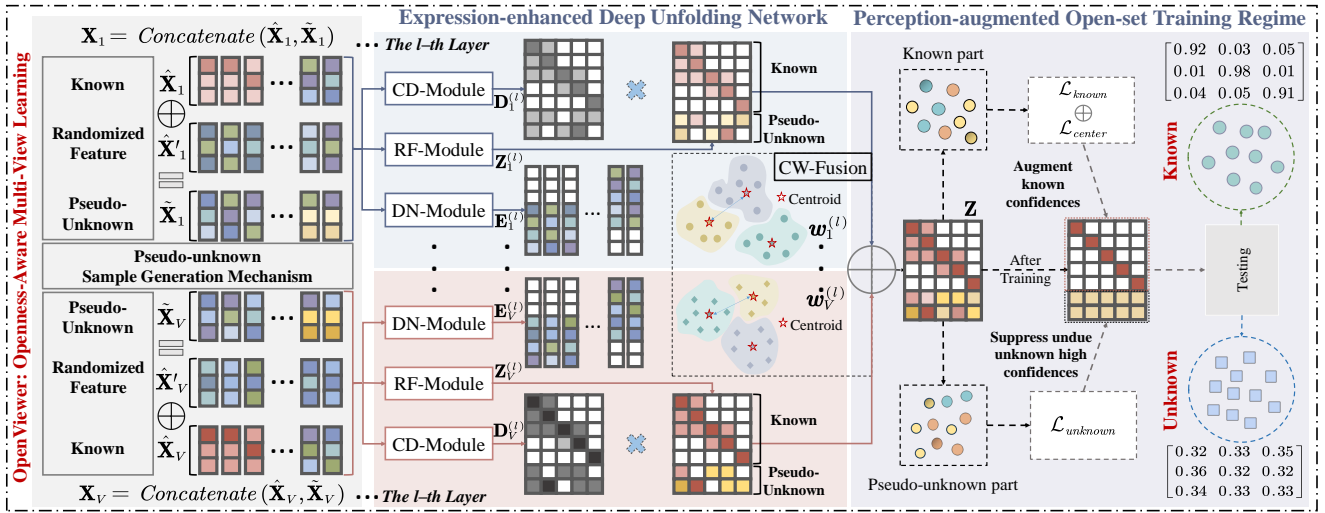


Figure 2: An overview of the proposed openness-aware multi-view learning framework (OpenViewer).

sion modules. The corresponding functions of each module are intuitively reflected in the prior-mapping optimization process, offering a more transparent integration mechanism. Additionally, we implement a multi-view sample perception-augmented open-set training regime to further boost confidences for known categories and suppress inappropriate confidences for unknown ones. This enables dynamic perception of known and unknown samples, thereby improving generalization. Finally, we present theoretical analysis and proof to substantiate OpenViewer’s ability to increase both interpretability and generalization. The main contributions of OpenViewer can be listed as follows:

- **Formulation of OpenViewer:** We propose OpenViewer, an openness-aware multi-view learning framework designed to tackle the challenges of interpretability and generalization, backed by theoretical guarantees.
- **Openness-aware models design:** We develop an interpretable expression-enhanced deep unfolding network, bolstered by a pseudo-unknown sample generation mechanism and a perception-augmented open-set training regime, to improve adaptation and generalization.
- **Extensive experiments on real-world datasets:** Experimental results validate OpenViewer’s effectiveness in addressing openness challenges, demonstrating superior recognition performance for both known and unknown.

Related Work

Two Multi-view Learning Methods. 1) **Heuristic methods** leverage multi-view prior knowledge to formulate and iteratively solve joint optimization objectives, leading to optimal multi-view learning solutions. For example, Wan *et al.* (Wan *et al.* 2023) proposed an auto-weighted multi-view optimization problem for large-scale data. Yu *et al.* (Yu *et al.* 2024a) devised a non-parametric joint optimization functions to partition multi-view data; 2) **Deep learning methods** utilize network architectures to automate the optimization of multi-view learning solutions and parameters. For ex-

ample, Xiao *et al.* (Xiao *et al.* 2023) performed multi-view deep learning by the consistency and complementarity. Xu *et al.* (Xu *et al.* 2024b) introduced the view-specific encoders and product-of-experts approach to aggregate multi-view information. Further work on multi-view learning can be discovered in (Chen *et al.* 2020; Wang *et al.* 2022; Yang *et al.* 2022; Liu *et al.* 2024) (heuristic) and (Yang *et al.* 2021; Lin *et al.* 2023; Du *et al.* 2024; Wang *et al.* 2024) (deep learning).

Interpretable Deep Unfolding Networks. Deep unfolding networks, derived from iterative solutions that encapsulate domain-specific priors and functional knowledge, have achieved success while maintaining strong interpretability across multiple fields (Gregor and LeCun 2010; Bonet *et al.* 2022; Zheng *et al.* 2023; Joukovsky, Eldar, and Deligiannis 2024). Some notable works, for example, Fu *et al.* (Fu *et al.* 2022) designed a model-driven deep unfolding structure for JPEG artifacts removal. Li *et al.* (Li *et al.* 2023) displayed a low-rank deep unfolding network for hyperspectral anomaly detection. Wu *et al.* (Wu *et al.* 2024) constructed a deep unfolding network based on first-order optimization algorithms. Additional similar efforts in deep unfolding networks can be traced in (Zhou *et al.* 2023; Weerdt, Eldar, and Deligiannis 2024; Fang *et al.* 2024b).

Open-set Learning. Open-set learning seeks to extend the closed-set hypothesis by equipping models with the ability to distinguish known and unknown classes. For instance, Dhamija *et al.* (Dhamija, Günther, and Boulton 2018) introduced the negative classes for improving the efficiency of unknown rejection. Duan *et al.* (Duan *et al.* 2023) formulated a subgraph-subgraph contrast to open-set graph learning into a multi-scale contrastive network. Safaei *et al.* (Safaei *et al.* 2024) explored an entropic open-set active learning framework to select informative unknown samples. Related open-set learning methods can also be found in (Bendale and Boulton 2016; Du *et al.* 2023; Gou *et al.* 2024).

Openness-Aware Multi-View Learning

| Notations | Descriptions |
|------------------------------------|--|
| V, C | The number of views and known classes. |
| N^o | The number of original training samples. |
| N^e | The number of pseudo-unknown training samples, $N^e \leq N^o$. |
| N | The number of total training samples, $N = N^o + N^e$. |
| D_v | The dimensions of the v -th view feature. |
| $\{\tilde{\mathbf{X}}_v\}_{v=1}^V$ | $\tilde{\mathbf{X}}_v \in \mathbb{R}^{N^o \times D_v}$ is the v -view original training samples. |
| $\{\tilde{\mathbf{X}}_v\}_{v=1}^V$ | $\tilde{\mathbf{X}}_v \in \mathbb{R}^{N^e \times D_v}$ is the v -view pseudo-unknown training samples. |
| $\{\mathbf{X}_v\}_{v=1}^V$ | $\mathbf{X}_v \in \mathbb{R}^{N \times D_v} = \text{Concatenate}(\tilde{\mathbf{X}}_v, \tilde{\mathbf{X}}_v)$ is the v -view training samples. |
| \mathbf{Y} | $\mathbf{Y} \in \{1, 2, \dots, C\}$ is the original training labels. |
| $\tilde{\mathbf{Y}}$ | $\tilde{\mathbf{Y}} \in \{C+1\}$ is the pseudo-unknown training labels. |
| \mathbf{Y} | $\mathbf{Y} \in \{1, 2, \dots, C, C+1\}$ is the total training labels. |
| $\{\mathbf{Z}_v\}_{v=1}^V$ | $\mathbf{Z}_v \in \mathbb{R}^{N \times C}$ is the v -th redundancy free representation. |
| $\{\mathbf{D}_v\}_{v=1}^V$ | $\mathbf{D}_v \in \mathbb{R}^{C \times D_v}$ is the v -th consistency dictionary learning matrix. |
| $\{\mathbf{E}_v\}_{v=1}^V$ | $\mathbf{E}_v \in \mathbb{R}^{N \times D_v}$ is the v -th diversity noise processing matrix. |
| $\{\mathbf{w}_v\}_{v=1}^V$ | \mathbf{w}_v is the v -th complementarity fusion contribution weight. |
| \mathbf{Z} | $\mathbf{Z} \in \mathbb{R}^{N \times C}$ is the complementarity enhanced representation. |
| \mathcal{D}_{train} | Multi-view training set, $\mathcal{D}_{train} = \mathcal{D}_{original} \cup \mathcal{D}_{generated}$. |
| $\mathcal{D}_{original}$ | Original training set, $\mathcal{D}_{original} = \{\{\tilde{\mathbf{X}}_v\}_{v=1}^V, \tilde{\mathbf{Y}}\}$. |
| $\mathcal{D}_{generated}$ | Pseudo-unknown training set, $\mathcal{D}_{generated} = \{\{\tilde{\mathbf{X}}_v\}_{v=1}^V, \tilde{\mathbf{Y}}\}$. |

Table 1: Essential notations and descriptions.

Pseudo-unknown Sample Generation Mechanism

The necessary notations are first listed in Table 1. To better tackle open-set environments, inspired by Mixup (Zhang et al. 2018), we utilize a pseudo-unknown sample generation mechanism to efficiently simulate open multi-view environments and previously adapt to potential unknown samples. Specifically, a perturbation parameter $\zeta \in [0, 1]$ is sampled from a $\zeta \sim \text{Beta}(\omega, \omega)$ distribution. Based on this, we randomly select $\hat{\mathbf{x}}_v^{(i)}$ and $\hat{\mathbf{x}}_v^{(j)}$ from the v -th view original feature $\tilde{\mathbf{X}}_v$, ensuring they belong to different categories. Then, the pseudo-unknown sample $\tilde{\mathbf{x}}_v$ is generated as

$$\tilde{\mathbf{x}}_v = \zeta \hat{\mathbf{x}}_v^{(i)} + (1 - \zeta) \hat{\mathbf{x}}_v^{(j)}, \quad (1)$$

where ζ determines the extent to which each original sample contributes to the features of the generated samples. Using Eq. (1), we generate a set of pseudo-unknown samples, $\mathcal{D}_{generated}$, and merge it with $\mathcal{D}_{original}$ to prepare the model for adapting to unknown classes.

Expression-enhanced Deep Unfolding Network

Subsequently, we design an interpretable expression-enhanced deep unfolding network to clarify the multi-view integration principle. We first abstract four multi-view functionalized priors as shown in Fig. 3, including: 1) **View-specific Redundancy** denotes the redundant similar features within each view; 2) **View-specific Consistency** indicates the dictionary coefficients, reflecting each representation's consistent contribution to the reconstruction of each view; 3) **View-specific Diversity** signifies the diverse noise information within each view; 4) **Cross-view Complementarity** refers to processed cross-view representations that can complementarity, enhance and express each other. Following that, we first consider the three view-specific priors, and construct a generalized expression-enhanced optimization problem as

$$\min_{\mathbf{Z}_v, \mathbf{D}_v, \mathbf{E}_v} \sum_{v=1}^V \left(\mathcal{I}(\mathbf{X}_v, \mathbf{Z}_v, \mathbf{D}_v, \mathbf{E}_v) + \alpha \Omega(\mathbf{Z}_v) + \beta \Psi(\mathbf{D}_v) + \gamma \Phi(\mathbf{E}_v) \right), \quad (2)$$

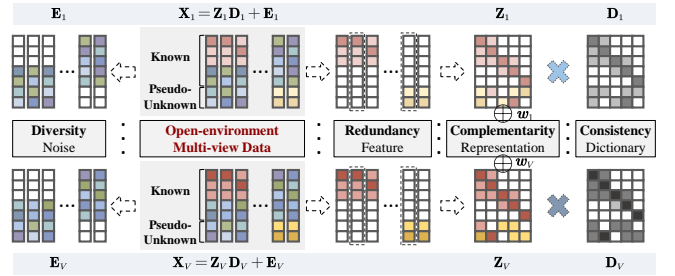


Figure 3: Four multi-view priors and their relationships.

where α, β, γ are the regularization parameters, and generalized Problem (2) includes the above functionalized priors that can be further concretized as

$$\min_{\mathbf{Z}_v, \mathbf{D}_v, \mathbf{E}_v} \sum_{v=1}^V \left(\frac{1}{2} \|\mathbf{X}_v - \mathbf{Z}_v \mathbf{D}_v - \mathbf{E}_v\|_F^2 + \alpha \|\mathbf{Z}_v\|_1 + \frac{\beta}{2} \|\mathbf{D}_v\|_F^2 + \gamma \|\mathbf{E}_v\|_{2,1} \right). \quad (3)$$

Problem (3) aims to learn a *redundancy* free representation \mathbf{Z}_v using l_1 -norm $\|\cdot\|_1$, while optimizing *consistency* dictionary coefficients \mathbf{D}_v and capturing *diversity* noise \mathbf{E}_v with the $l_{2,1}$ -norm $\|\cdot\|_{2,1}$. So \mathbf{X}_v can be expressed as a linear combination $\mathbf{Z}_v \mathbf{D}_v + \mathbf{E}_v$. To optimize such a mixed non-convex problem (3) consisting of smooth terms $\mathcal{I}(\cdot)$, $\Psi(\cdot)$ and non-smooth terms $\Omega(\cdot)$, $\Phi(\cdot)$, ADMM (Boyd et al. 2011) is employed to decompose it into three sub-problems for solving. For $\mathbf{Z}_v = \{\hat{\mathbf{Z}}_v, \tilde{\mathbf{Z}}_v\}$, $\mathbf{E}_v = \{\hat{\mathbf{E}}_v, \tilde{\mathbf{E}}_v\}$, $\mathbf{D}_v = \{\hat{\mathbf{D}}_v, \tilde{\mathbf{D}}_v\}$ sub-problems, where $\hat{\mathbf{Z}}_v, \hat{\mathbf{E}}_v$, and $\hat{\mathbf{D}}_v$ are known, and $\tilde{\mathbf{Z}}_v, \tilde{\mathbf{E}}_v$, and $\tilde{\mathbf{D}}_v$ are pseudo-unknown, we utilize proximal gradient descent method (Beck and Teboulle 2009) to solve \mathbf{Z}_v and \mathbf{E}_v variables, while \mathbf{D}_v variable has a closed-form solution, obtained as

$$\begin{aligned} \mathbf{Z}_v^{(l+1)} &\leftarrow \mathcal{S}_{\frac{\alpha}{L_{pv}}} \left(\mathbf{Z}_v^{(l)} - \frac{1}{L_{pv}} \nabla \mathcal{I}(\mathbf{Z}_v^{(l)}) \right), \\ \mathbf{E}_v^{(l+1)} &\leftarrow \mathcal{P}_{\frac{\gamma}{L_{pv}}} \left(\mathbf{E}_v^{(l)} - \frac{1}{L_{pv}} \nabla \mathcal{I}(\mathbf{E}_v^{(l)}) \right), \\ \mathbf{D}_v^{(l+1)} &\leftarrow \{ \nabla \mathcal{I}(\mathbf{D}_v^{(l)}) + \nabla \Psi(\mathbf{D}_v^{(l)}) = 0 \}, \end{aligned} \quad (4)$$

where $\mathcal{S}_{\frac{\alpha}{L_{pv}}}(\cdot)$ and $\mathcal{P}_{\frac{\gamma}{L_{pv}}}(\cdot)$ are the redundancy and diversity proximal operators, respectively. $\nabla(\cdot)$ denotes the gradient of the current variable, L_{pv} is the v -th Lipschitz constant of $\nabla \mathcal{I}(\cdot)$, and l is the current iteration. Subsequently, we expand the gradient-related notations, detailed as

$$\begin{cases} \mathbf{Z}_v^{(l+1)} &\leftarrow \mathcal{S}_{\frac{\alpha}{L_{pv}}} \left(\mathbf{Z}_v^{(l)} - \frac{1}{L_{pv}} \left(\mathbf{Z}_v^{(l)} \mathbf{D}_v^{(l)} (\mathbf{D}_v^{(l)\top})^{(l)} - \mathbf{X}_v (\mathbf{D}_v^{(l)\top})^{(l)} + \mathbf{E}_v^{(l)} (\mathbf{D}_v^{(l)\top})^{(l)} \right) \right) \\ &\Rightarrow \mathcal{S}_{\frac{\alpha}{L_{pv}}} \left(\mathbf{Z}_v^{(l)} \left(\mathbf{I} - \frac{1}{L_{pv}} \mathbf{D}_v^{(l)} (\mathbf{D}_v^{(l)\top})^{(l)} \right) + \frac{1}{L_{pv}} (\mathbf{X}_v - \mathbf{E}_v^{(l)}) (\mathbf{D}_v^{(l)\top})^{(l)} \right), \\ \mathbf{D}_v^{(l+1)} &\leftarrow \left((\mathbf{Z}_v^{(l+1)\top}) \mathbf{Z}_v^{(l+1)} + \beta \mathbf{I} \right)^{-1} (\mathbf{Z}_v^{(l+1)\top})^{(l+1)} (\mathbf{X}_v - \mathbf{E}_v^{(l)}), \\ \mathbf{E}_v^{(l+1)} &\leftarrow \mathcal{P}_{\frac{\gamma}{L_{pv}}} \left(\mathbf{X}_v - \mathbf{Z}_v^{(l+1)} \mathbf{D}_v^{(l+1)} \right), \end{cases} \quad (5)$$

where $\mathbf{I} \in \mathbb{R}^{C \times C}$ is an identity matrix. Thus far, we have used the ADMM optimizer to solve the corresponding sub-problems and derive iterative solutions for *redundancy, consistency, diversity* priors. Then, an inter-class discretion-guided weighting method is applied to account for the cross-view *complementary* prior. Intuitively, the closer the sample centroids are within a view, the less complementary information each view provides. Based on this, we dynamically perceive the centroid as $\mathbf{o}_v^{(i)} = \frac{1}{|B_i|} \sum_{j: Y_j=i} \mathbf{z}_v^{(j)}$ and

then calculate the inter-class distances between all centroids for each view, where $|B_i|$ is the number of training instances in category i . To prevent the largest distance between two classes from overly influencing the measure of inter-class discrepancy, we focus on the minimum distance \mathbf{d}_v between any two categories, defined as $\mathbf{d}_v = \min \left\{ \text{Dist} \left(\mathbf{o}_v^{(i)}, \mathbf{o}_v^{(j)} \right) \right\}, i, j \in \mathbf{Y}$ and $i \neq j$. Here, $\text{Dist}(\cdot, \cdot)$ is the distance function, which in this work is the Euclidean distance. This strategy provides a balanced assessment of the complementary contribution of different views. The higher the complementarity information between views (*i.e.*, the greater the distance between centroids), the greater their assigned weights, denoted as

$$\mathbf{w}_v = \frac{\exp(-\bar{\mathbf{d}}_v)}{\sum_{v=1}^V \exp(-\bar{\mathbf{d}}_v)}, \bar{\mathbf{d}}_v = \mathbf{d}_v^{-1} / \|\mathbf{d}_v^{-1}\|_1, \sum_{v=1}^V \mathbf{w}_v = 1, \quad (6)$$

where $\bar{\mathbf{d}}_v$ is obtained by normalizing the inverse of \mathbf{d}_v between centroids through ℓ_1 -norm. At last, the inter-class discretion-guided weights $\{\mathbf{w}_v\}_{v=1}^V$ can be applied to perform complementary fusion $\mathcal{F}(\cdot)$ as

$$\mathbf{Z}^{(l+1)} \leftarrow \sum_{v=1}^V \mathbf{w}_v^{(l+1)} \mathbf{Z}_v^{(l+1)}. \quad (7)$$

Based on solutions (4) and (7), the multi-view feature expression-enhanced deep unfolding network can be conceptualized as four interpretable prior-mapping modules by parameterizing alternative components (Zhou et al. 2023; Weerdt, Eldar, and Deligiannis 2024) as

$$\begin{cases} \text{RF-Module: } \mathbf{Z}_v^{(l+1)} & \leftarrow \mathcal{S}_{\theta_v^{(l)}} \left(\mathbf{Z}_v^{(l)} \mathbf{R} + (\mathbf{X}_v - \mathbf{E}_v^{(l)}) (\mathbf{D}_v^\top)^{(l)} \mathbf{U} \right), \\ \text{CD-Module: } \mathbf{D}_v^{(l+1)} & \leftarrow \mathbf{M} (\mathbf{Z}_v^\top)^{(l+1)} (\mathbf{X}_v - \mathbf{E}_v^{(l)}), \\ \text{DN-Module: } \mathbf{E}_v^{(l+1)} & \leftarrow \mathcal{P}_{\rho_v^{(l)}} \left(\mathbf{X}_v - \mathbf{Z}_v^{(l+1)} \mathbf{D}_v^{(l+1)} \right), \\ \text{CW-Fusion: } \mathbf{Z}^{(l+1)} & \leftarrow \sum_{v=1}^V \mathbf{w}_v^{(l+1)} \mathbf{Z}_v^{(l+1)}, \end{cases} \quad (8)$$

where $\mathbf{R} = \mathbf{I} - \frac{1}{L_{p_v}} \mathbf{D}_v \mathbf{D}_v^\top$, $\mathbf{U} = \frac{1}{L_{p_v}} \mathbf{I}$, and $\mathbf{M} = (\mathbf{Z}_v^\top \mathbf{Z}_v + \beta \mathbf{I})^{-1}$. The learnable redundancy and diversity proximal operators $\mathcal{S}_{\theta_v^{(l)}}(\cdot)$ and $\mathcal{P}_{\rho_v^{(l)}}(\cdot)$ are the reparameterized versions of $\mathcal{S}_{\frac{\alpha}{L_{p_v}}}(\cdot)$ and $\mathcal{P}_{\frac{\gamma}{L_{p_v}}}(\cdot)$, with learnable threshold parameters θ_v and ρ_v , respectively. Moreover, $\mathcal{S}_{\theta_v}(\mathbf{a}^{(ij)}) = \sigma(\mathbf{a}^{(ij)} - \theta_v) - \sigma(-\mathbf{a}^{(ij)} - \theta_v)$, and $\mathcal{P}_{\rho_v}(\mathbf{a}^{(i)}) = \frac{\sigma(\|\mathbf{a}^{(i)}\|_2 - \rho_v)}{\|\mathbf{a}^{(i)}\|_2} \mathbf{a}^{(i)}$, if $\rho_v < \|\mathbf{a}^{(i)}\|_2$; otherwise,

0. $\mathbf{a}^{(ij)}$ is the element in the i -th row and j -th column of the matrix, $\mathbf{a}^{(i)}$ is the i -th column of the matrix, and $\sigma(\cdot)$ can be activation functions such as ReLU, SeLU and etc.

The constructed network, incorporating these modules, can engage in multi-view expression enhancement while integrating their functions into deep networks to maintain interpretability: 1) **Redundancy Free Representation Module (RF-Module)** introduces learnable layers and redundancy-free operators to reduce redundant features and retain the most critical view information \mathbf{Z}_v ; 2) **Consistency Dictionary Learning Module (CD-Module)** captures dictionary coefficients \mathbf{D}_v within each view, denoting the consistent contribution of each \mathbf{Z}_v to the reconstruction of \mathbf{X}_v ; 3) **Diversity Noise Processing Module (DN-Module)** develops learnable diversity operators to eliminate irrelevant information \mathbf{E}_v caused by the noise or outliers; 4) **Complementarity Fusion Representation Module (CW-Fusion)** implements complementary weight fusion to integrate representations as \mathbf{Z} to differentiate between known and unknown. Unfolding network (8) is composed of L layers, with each layer corresponding to a single ADMM iteration. The interpretability is reflected in the optimization process: 1) For multi-view known parts, it enhances expression by processing noise and integrating complementary; 2) For multi-view unknown parts, it employs redundancy removal, noise processing, and adapts to a pseudo-unknown dictionary to highlight inappropriate unknown confidences. This enhanced expression provides a solid foundation for distinguishing between known and unknown, thereby boosting OpenViewer’s interpretability and trustworthiness.

Perception-augmented Open-set Training Regime

The above interpretable network has performed feature-level integration and enhancement. Subsequently, we design a loss regime to further augment sample-level perception and improve the model’s generalization. For known samples, we first ensure the model’s ability to recognize them by applying a cross-entropy loss. Building on this, we promote the separation of all known classes by a distance margin term $\max(\boldsymbol{\xi} - \|\hat{\mathbf{z}}^{(i)}\|_2, 0)^2$, formalized as

$$\begin{aligned} \mathcal{L}_{known} &= -\frac{1}{N^o} \sum_{i=1}^{N^o} \sum_{c=1}^C \left(\hat{\mathbf{y}}_c^{(i)} \log P(c | \hat{\mathbf{z}}^{(i)}) \right) \\ &+ \sum_{i=1}^{N^o} \max(\boldsymbol{\xi} - \|\hat{\mathbf{z}}^{(i)}\|_2, 0)^2, \end{aligned} \quad (9)$$

where $\hat{\mathbf{z}}^{(i)} \in \hat{\mathbf{Z}}$, P is the Softmax score, and $\boldsymbol{\xi}$ is the distance margin. In this way, the feature vector is pushed out of the margin $\boldsymbol{\xi}$ to make its norm as close to or greater than $\boldsymbol{\xi}$ as possible, thereby augmenting the discrimination between known class samples. For the more critical unknown part, we aim to minimize the allocation of pseudo-unknown samples to known groups. Therefore, we employ a ℓ_2 -norm regularization term $\|\tilde{\mathbf{z}}^{(i)}\|_2^2$ to ensure that OpenViewer suppresses excessive unknown high confidences, expressed as

$$\mathcal{L}_{unknown} = -\frac{1}{C} \sum_{i=1}^{N^e} \sum_{c=1}^C \left(\log P(c | \tilde{\mathbf{z}}^{(i)}) \right) + \sum_{i=1}^{N^e} \|\tilde{\mathbf{z}}^{(i)}\|_2^2, \quad (10)$$

where $\tilde{z}^{(i)} \in \tilde{\mathbf{Z}}$, and $P(c | \tilde{z}^{(i)})$ is the probability that the model predicts the pseudo-unknown sample $\tilde{z}^{(i)}$ as belonging to category c . Loss (10) ensures that the model’s prediction confidence for each known class is average and penalizes pseudo-unknown that are close to known, thereby suppressing inappropriate confidences for unknown samples.

However, the above loss only increases the inter-class separability between known and unknown samples. To promote intra-class compactness, we use the following center loss to further separate the feature vectors of different classes as

$$\mathcal{L}_{center} = \frac{1}{2} \sum_{i=1}^{N^o} \left\| \tilde{z}_c^{(i)} - \mathbf{c}^{\hat{y}_c^{(i)}} \right\|_2^2, \quad (11)$$

where $\mathbf{c}^{\hat{y}_c^{(i)}}$ is the center vector corresponding to the i -th sample’s true label. Then, each category center is dynamically updated during training to better reflect the sample distribution of its corresponding category, described as

$$\Delta \mathbf{c}^{(j) \in C} = \frac{\sum_{i=1}^{N^o} \delta(\hat{y}_c^{(i)} = j) \cdot (\mathbf{c}^{(j)} - \tilde{z}_c^{(i)})}{1 + \sum_{i=1}^{N^o} \delta(\hat{y}_c^{(i)} = j)}, \quad (12)$$

where $\Delta \mathbf{c}^{(j) \in C}$ the update amount for the center of category j , $\delta(\cdot)$ is an indicator function that takes the value 1 when the i -th sample belongs to category j ; otherwise, 0. Meanwhile, the center vectors of each class are adjusted by the calculated update amounts as $\hat{\mathbf{c}}_{new}^{(i)} \leftarrow \hat{\mathbf{c}}_{old}^{(i)} - \Delta \mathbf{c}^{(j)}$, where $\hat{\mathbf{c}}_{new}^{(i)}$ is the updated center vectors, while $\hat{\mathbf{c}}_{old}^{(i)}$ is the old center vectors.

At last, we train the unfolding network (8) by combining these losses to augment perception as

$$\mathcal{L}_{total} = \mathcal{L}_{known} + \lambda_1 \mathcal{L}_{unknown} + \lambda_2 \mathcal{L}_{center}, \quad (13)$$

where λ_1 and λ_2 are two trade-off parameters. The contribution of training regime (13) to OpenViewer’s generalization is twofold: 1) From a feature correspondence perspective, it ensures that known parts elicit a strong response, while undue confidences of pseudo-unknown are suppressed to a low response; 2) From an entropy perspective, it reduces the entropy of known to augment discrimination, while increasing the entropy of pseudo-unknown to ensure that they have low confidence in being classified as known, thereby further reinforcing the recognition of unknown. OpenViewer can be summarized as Algorithm 1 in **Appendix**.

Main Theoretical Presentation and Analysis

Theorem 1. (Interpretability Boundary) *If each submodule is convergent, then the stacked deep unfolding network consisting of all modules is bounded.*

Remark 1. Supported by **Theorem 1**, the interpretable deep unfolding network (8) will be bounded regardless of the initial multi-view cases with known and pseudo-unknown, indicating that information from different views can be reasonably integrated and **interpreted** in mixed scenarios, thereby improving the trustworthiness.

Theorem 2. (Generalization Support) *For the fixed step size (i.e., $\eta_t = \eta$) as $T \rightarrow \infty$, and given the existing upper boundary ϵ , the difference $\mathcal{L}_T^* - \mathcal{L}^*$ generalizes to $\frac{\eta \epsilon^2}{2}$ with a convergence rate $\mathcal{O}(1/T)$.*

| Datasets | # Samples | # Views | # Feature Dimensions | # Classes |
|-------------|-----------|---------|-----------------------------------|-----------|
| Animals | 10,158 | 2 | 4,096/4,096 | 50 |
| AWA | 30,475 | 6 | 2,688/2,000/252/2,000/2,000/2,000 | 50 |
| NUSWIDEOBJ | 30,000 | 5 | 65/226/145/74/129 | 31 |
| VGGFace2-50 | 34,027 | 4 | 944/576/512/640 | 50 |
| ESP-Game | 11,032 | 2 | 100/100 | 7 |
| NUSWIDE20k | 20,000 | 2 | 100/100 | 8 |

Table 2: A brief description of the tested datasets.

Remark 2. Theorem 2 theoretically ensures that OpenViewer maintains stable **generalization** by learning a true distribution within a convergence radius of $\frac{\eta \epsilon^2}{2}$ and a convergence rate $\mathcal{O}(1/T)$, even when encountering unknown.

Complexity. The time complexity of OpenViewer with L layers costs $\mathcal{O}((NC(C + D_v + V) + C^2 D_v) L)$, and the space complexity of OpenViewer denotes $\mathcal{O}(N(D_v + C)V)$. Additional proofs and details of the main theories and complexity can be found in **Appendix**.

Experiments and Studies

Datasets, Compared Methods, and Evaluation Metric.

We conduct experiments in challenging open-environment classification tasks under six well-known multi-view datasets. This includes two scenarios: 1) Animals, AWA, NUSWIDEOBJ, and VGGFace2-50 datasets contain different manual and deep features; 2) ESP-Game and NUSWIDE20k datasets include various vision and language features. The statistics of these datasets are summarized in Table 2 (details in **Appendix**). Moreover, to simulate the performance of OpenViewer in open-environment, we also utilize the concept of **openness** (Scheirer et al. 2012) to divide known and unknown categories of multi-view datasets. Meanwhile, the dataset is partitioned as follows: 10% of the known class samples are allocated for training, another 10% for validation, and the rest 80% for testing.

Due to the limited exploration of related open multi-view learning tasks, we drew on backbone networks from other different multi-view tasks as compared methods (details in **Appendix**), including: MvNNcor (Xu et al. 2020), TMC (Han et al. 2021), MMDynamics (Han et al. 2022), IMvGCN (Wu et al. 2023), LGCN-FF (Chen et al. 2023), ORLNet (Fang et al. 2024a), and RCML (Xu et al. 2024a).

To estimate recognition performance effectively, the Open-Set Classification Rate (OSCR) (Dhamija, Günther, and Boulton 2018) is adopted as metrics, consisting of Correct Classification Rate (CCR) and False Positive Rate (FPR).

Experimental Setups. OpenViewer is implemented using the PyTorch on an NVIDIA GeForce RTX 4080 GPU with 16GB of memory. We train OpenViewer for 100 epochs with a batch size of 50, a learning rate of 0.01, $\xi = 5$, and λ_1 and λ_2 selected from $\{10^{-3}, 5 \times 10^{-3}, \dots, 10^0\}$. The number of unfolding layers is set to $L = 1$ as suggested in **Appendix** Fig. 3, balancing complexity and efficiency while preserving interpretable expression-enhanced capabilities. The ablation-models (**Appendix** Table 1) are OpenSViewer (w/o CD-Module and DN-Module) and OpenSDViewer (w/o DN-Module) using for self-verification.

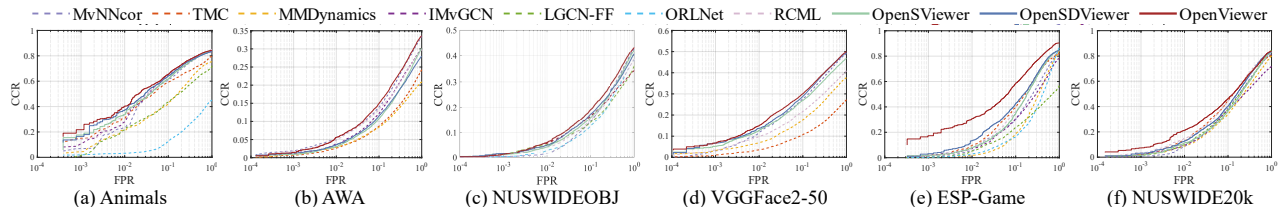


Figure 4: OSCR curves plotting the CCR over FPR on all test multi-view datasets for all compared methods.

| Datasets | Animals | | | | | AWA | | | | | NUSWIDEOBJ | | | | |
|------------------------------|--------------|--------------|--------------|--------------|--------------|-------------|-------------|--------------|--------------|--------------|-------------|-------------|--------------|--------------|--------------|
| | 0.5% | 1.0% | 5.0% | 10% | 50% | 0.5% | 1.0% | 5.0% | 10% | 50% | 0.5% | 1.0% | 5.0% | 10% | 50% |
| MvNNcor (Xu et al. 2020) | 19.48 | 23.35 | 53.81 | 61.01 | 79.30 | 1.59 | 2.15 | 6.40 | 9.34 | 23.07 | 0.82 | 1.63 | 9.34 | 14.48 | 33.40 |
| TMC (Han et al. 2021) | 24.30 | 30.36 | 51.22 | 59.25 | 72.04 | 1.67 | 2.60 | 6.09 | 8.68 | 18.05 | 4.17 | <u>5.29</u> | 10.45 | 14.07 | 27.28 |
| MMDynamics (Han et al. 2022) | 16.93 | 21.51 | 35.65 | 42.39 | 69.11 | 1.78 | 2.75 | 7.04 | 9.86 | 20.19 | 3.39 | 5.10 | <u>12.58</u> | <u>17.72</u> | 30.59 |
| IMvGCN (Wu et al. 2023) | 21.44 | 27.73 | 56.08 | 63.54 | 78.57 | 1.21 | 1.80 | 4.03 | 5.89 | 12.38 | 0.44 | 0.88 | 3.15 | 4.78 | 9.76 |
| LGCN-FF (Chen et al. 2023) | 15.18 | 21.40 | 34.37 | 43.59 | 63.53 | - | - | - | - | - | - | - | - | - | - |
| ORLNet (Fang et al. 2024a) | 10.76 | 12.46 | 23.08 | 31.71 | 49.81 | - | - | - | - | - | - | - | - | - | - |
| RCML (Xu et al. 2024a) | 25.31 | 33.38 | 55.48 | 63.87 | <u>80.03</u> | 3.52 | <u>4.75</u> | <u>10.11</u> | <u>13.34</u> | <u>24.69</u> | 2.99 | 4.26 | 10.44 | 15.22 | 30.19 |
| OpenSViewer | 27.64 | 33.83 | 53.50 | 61.75 | 79.54 | 2.34 | 3.09 | 7.55 | 10.77 | 23.30 | 3.02 | 4.37 | 11.41 | 16.08 | 32.64 |
| OpenSDViewer | <u>30.98</u> | <u>37.05</u> | <u>56.47</u> | <u>64.21</u> | 79.61 | 2.36 | 3.56 | 8.09 | 11.49 | 23.54 | 3.60 | 5.02 | 12.47 | 17.43 | <u>32.80</u> |
| OpenViewer | 31.56 | 40.24 | 58.07 | 65.38 | 80.78 | <u>3.49</u> | 5.59 | 11.08 | 14.97 | 27.66 | <u>4.12</u> | 6.16 | 14.17 | 19.12 | 35.19 |

| Datasets | VGGFace2-50 | | | | | ESP-Game | | | | | NUSWIDE20k | | | | |
|------------------------------|--------------|--------------|--------------|--------------|--------------|--------------|--------------|--------------|--------------|--------------|--------------|--------------|--------------|--------------|--------------|
| | 0.5% | 1.0% | 5.0% | 10% | 50% | 0.5% | 1.0% | 5.0% | 10% | 50% | 0.5% | 1.0% | 5.0% | 10% | 50% |
| MvNNcor (Xu et al. 2020) | 8.29 | 11.65 | 22.31 | 27.53 | 43.01 | 3.48 | 5.72 | 21.48 | 30.15 | 68.22 | 2.90 | 8.24 | 26.59 | 38.69 | 70.62 |
| TMC (Han et al. 2021) | 2.55 | 3.57 | 8.07 | 10.72 | 20.87 | 6.25 | 9.33 | 28.70 | 40.05 | 74.45 | 8.30 | 13.21 | <u>33.04</u> | <u>44.72</u> | 73.35 |
| MMDynamics (Han et al. 2022) | 5.55 | 6.91 | 13.70 | 17.62 | 31.53 | 0.99 | 1.52 | 8.92 | 18.71 | 64.20 | 5.67 | 8.77 | 24.63 | 33.88 | 66.16 |
| IMvGCN (Wu et al. 2023) | - | - | - | - | - | 4.69 | 7.10 | 20.84 | 30.65 | 62.34 | 9.15 | 11.65 | 24.88 | 35.97 | 63.42 |
| LGCN-FF (Chen et al. 2023) | - | - | - | - | - | 2.18 | 5.07 | 15.56 | 23.84 | 45.17 | - | - | - | - | - |
| ORLNet (Fang et al. 2024a) | - | - | - | - | - | 1.65 | 2.61 | 11.26 | 16.67 | 56.48 | 6.10 | 9.85 | 27.08 | 37.55 | 70.72 |
| RCML (Xu et al. 2024a) | 7.85 | 9.85 | 17.21 | 21.64 | 34.60 | 4.62 | 7.77 | 24.31 | 36.25 | 75.91 | <u>10.16</u> | <u>14.94</u> | 31.61 | 44.29 | <u>73.37</u> |
| OpenSViewer | 10.18 | 12.77 | 21.80 | 26.86 | 40.82 | 4.66 | 8.16 | 21.94 | 34.91 | 75.24 | 6.49 | 11.26 | 25.55 | 36.39 | 70.66 |
| OpenSDViewer | <u>10.75</u> | <u>13.75</u> | <u>23.23</u> | <u>28.80</u> | <u>43.28</u> | <u>7.96</u> | <u>13.35</u> | <u>30.92</u> | <u>42.56</u> | <u>76.76</u> | 7.89 | 12.67 | 28.84 | 40.34 | 72.56 |
| OpenViewer | 12.16 | 15.05 | 25.39 | 30.05 | 44.14 | 25.89 | 30.61 | 46.45 | 58.65 | 83.52 | 16.35 | 21.31 | 36.76 | 46.28 | 73.47 |

Table 3: CCR at different FPR is given for all comparison under *openness* = 0.1 setting, where the best and runner-up results are highlighted in **boldface** and underlined, respectively. “-” indicates the out-of-memory error.

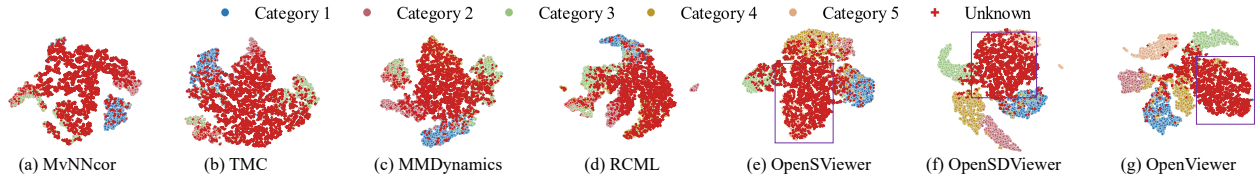


Figure 5: The t-SNE visualizations based on the fused representations of ESP-Game dataset.

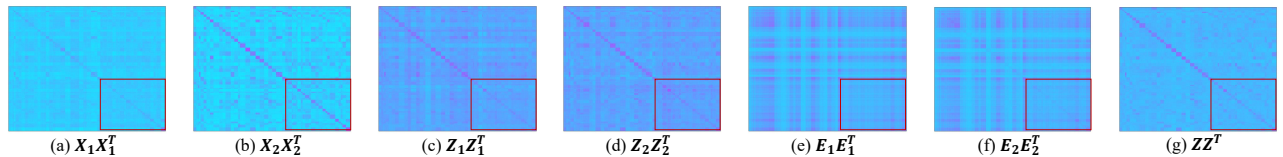


Figure 6: The heatmaps on feature, redundancy-free, noise and fusion matrices with $w_1 = 0.5132$ and $w_2 = 0.4868$ of Animals.

Experimental Results. We present the overall OSCR curve results of all multi-view learning methods in classification under the condition of *openness* = 0.1, as shown in Fig. 4, from which we observe: Intuitively, OpenViewer (red solid line) outperforms other methods (colored dashed lines) across all cases, whether on multi-feature or multi-modal

datasets. Although some multi-view methods, such as TMC and RCML, occasionally outperform OpenViewer in specific cases, it demonstrates more stable performance across all scenarios. Finally, OpenViewer’s effective balance across different FPR and CCR results in outstanding performance. On one hand, this may be attributed to the effective enhance-

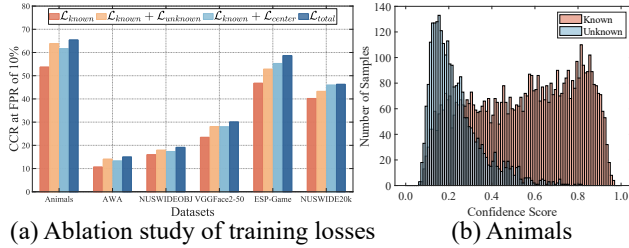


Figure 7: Ablation study of training losses on multi-view datasets with respect to CCR at FPR of 10%.

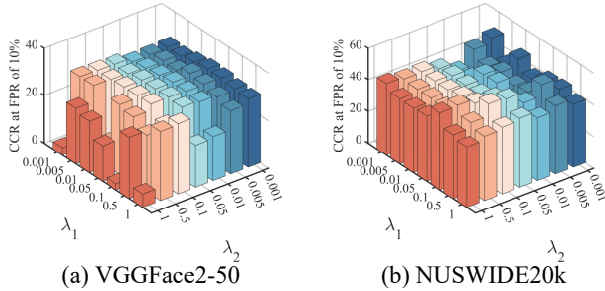


Figure 8: Parameter sensitivity of λ_1 and λ_2 .

ment of both known and unknown expression through interpretable integration, such as the multi-feature expression enhancement seen with VGGFace2-50. On the other hand, the pseudo-unknown mechanism and perception-augmented loss contribute to significant confidence differentiation, as depicted in Fig. 6 (g) for Animals.

Meanwhile, we further extract representative **CCR at FPR of 0.5%/1.0%/5.0%/10.0%/50.0%** and illustrate them in Table 3. It is evident that OpenViewer surpasses other methods in most cases, particularly under high FPR conditions (e.g., 50.0%). Moreover, Fig. 5 (all in **Appendix Fig. 1**) indicates that OpenViewer achieves the highest separation between different categories and minimal overlap between unknown and known categories. Additionally, Fig. 6 clearly demonstrates the impact of functionalized priors in OpenViewer. Original features exhibit complementary information but also contain redundancy, noise, and inappropriate confidences. Whereas OpenViewer effectively filters relevant features and noise, and suppresses inappropriate confidences for unknown (the red box). Ultimately, the weight-guided complementary fusion effectively enhances expression with a clean diagonalized structure, revealing high response for known and low response for unknown.

Ablation Study. To verify that each module and loss term contributes to address openness challenges, we conduct ablation experiments. First, when we comprehensively examine the variants OpenSViewer, OpenSDViewer, and OpenViewer portrayed in Fig. 4, Fig. 5 (**Appendix Fig. 1**), and Table 3, we can excitedly discover that the addition of each interpretable module promotes performance improvement and effective separation of samples. For example, after adding the diversity noise processing module (DN-

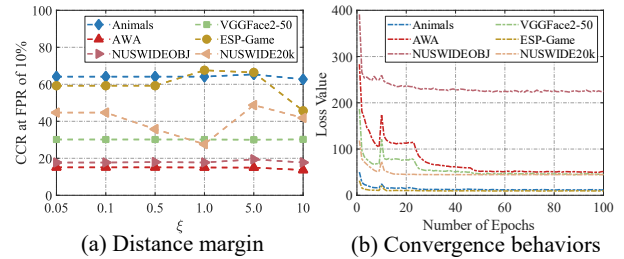


Figure 9: Parameter sensitivity of ξ and loss behaviors.

Module), the performance of ESP-Game improved from 42.56% to 58.65%, with increased inter-class separability between known and unknown. This improvement can be attributed to the removal of multi-view noise, which enhances feature expression. Furthermore, Fig. 7 (a) progressively highlights the generalized contributions of all loss components. From this, their combination can promote the model’s generalization by distinguishing between normal known and undue unknown confidences. Taking the Animals dataset as an example, Fig. 7 (b) depicts that training regime accentuates differences in confidence scores between known and unknown distributions, aiding in recognition. Specifically, the unknown loss enhances sample discrimination, while the center loss promotes intra-class compactness.

Parameter Sensitivity Analysis. First, Fig. 8 (all in **Appendix Fig. 4**) illustrates the parameter sensitivity of OpenViewer on two representative datasets in terms of λ_1 and λ_2 of loss (13). The model performance is generally robust in most cases, but it collapses when λ_2 becomes too large, causing all samples to provide meaningless confidences across all classes, with no clear winning class. Second, Fig. 9 (a) reveals when the parameter ξ is set to 5, the feature range is adequate to effectively distinguish. However, when this value is exceeded, the wider feature range causes overlap among known classes, leading to a decline in overall performance. Finally, we showcase Fig. 9 (b) to elucidate the behaviors between loss values and training epochs. The curve displays that after 100 training epochs, the loss value stabilizes, indicating convergence and underscoring its stability, as depicted in **Theoretical Analysis**.

Conclusion and Future Work

In this paper, we proposed OpenViewer to address the openness challenges in open-settings. OpenViewer began with a pseudo-unknown sample generation mechanism to previously adapt to unknown, followed by a multi-view expression-enhanced deep unfolding network to offer a more interpretable integration mechanism. Additionally, OpenViewer employed a perception-augmented open-set training regime to improve generalization between known and unknown classes. Extensive experiments on diverse multi-view datasets showed that OpenViewer outperformed existing methods in recognition while effectively tackling openness challenges. In future work, we will explore more sophisticated openness-aware circumstances based multi-view learning, including heterogeneous or incomplete data.

References

- Beck, A.; and Teboulle, M. 2009. A fast iterative shrinkage-thresholding algorithm for linear inverse problems. *SIAM Journal on Imaging Sciences*, 2(1): 183–202.
- Bendale, A.; and Boulton, T. E. 2016. Towards open set deep networks. In *Proceedings of the IEEE Conference on Computer Vision and Pattern Recognition*, 1563–1572.
- Bonet, E. R.; Do, T. H.; Qin, X.; Hofman, J.; Manna, V. P. L.; Philips, W.; and Deligiannis, N. 2022. Explaining graph neural networks with topology-aware node selection: Application in air quality inference. *IEEE Transactions on Signal and Information Processing over Networks*, 8: 499–513.
- Boyd, S.; Parikh, N.; Chu, E.; Peleato, B.; Eckstein, J.; et al. 2011. Distributed optimization and statistical learning via the alternating direction method of multipliers. *Foundations and Trends® in Machine Learning*, 3(1): 1–122.
- Chen, M.; Huang, L.; Wang, C.-D.; and Huang, D. 2020. Multi-view clustering in latent embedding space. In *Proceedings of the Thirty-Fourth AAAI Conference on Artificial Intelligence*, 3513–3520.
- Chen, Z.; Fu, L.; Yao, J.; Guo, W.; Plant, C.; and Wang, S. 2023. Learnable graph convolutional network and feature fusion for multi-view learning. *Information Fusion*, 95: 109–119.
- Dhamija, A. R.; Günther, M.; and Boulton, T. 2018. Reducing network agnostophobia. In *Advances in Neural Information Processing Systems*, 1–12.
- Du, S.; Cai, Z.; Wu, Z.; Pi, Y.; and Wang, S. 2024. UMCGL: Universal multi-view consensus graph learning with consistency and diversity. *IEEE Transactions on Image Processing*, 33: 3399–3412.
- Du, S.; Fang, Z.; Lan, S.; Tan, Y.; Günther, M.; Wang, S.; and Guo, W. 2023. Bridging trustworthiness and open-world learning: An exploratory neural approach for enhancing interpretability, generalization, and robustness. In *Proceedings of the Thirty-First ACM International Conference on Multimedia*, 8719–8729.
- Duan, J.; Wang, S.; Zhang, P.; Zhu, E.; Hu, J.; Jin, H.; Liu, Y.; and Dong, Z. 2023. Graph anomaly detection via multi-scale contrastive learning networks with augmented view. In *Proceedings of the Thirty-Seventh AAAI Conference on Artificial Intelligence*, 7459–7467.
- Fang, Z.; Du, S.; Cai, Z.; Lan, S.; Wu, C.; Tan, Y.; and Wang, S. 2024a. Representation learning meets optimization-derived networks: From single-view to multi-view. *IEEE Transactions on Multimedia*, 26: 8889–8901.
- Fang, Z.; Du, S.; Chen, Y.; and Wang, S. 2024b. Beyond the known: Ambiguity-aware multi-view learning. In *Proceedings of the Thirty-Second ACM International Conference on Multimedia*, 8518–8526.
- Fu, X.; Wang, M.; Cao, X.; Ding, X.; and Zha, Z. 2022. A model-driven deep unfolding method for JPEG artifacts removal. *IEEE Transactions on Neural Networks and Learning Systems*, 33(11): 6802–6816.
- Gou, Y.; Zhao, H.; Li, B.; Xiao, X.; and Peng, X. 2024. Test-Time degradation adaptation for open-set image restoration. In *Proceedings of the Forty-First International Conference on Machine Learning*, 1–11.
- Gregor, K.; and LeCun, Y. 2010. Learning fast approximations of sparse coding. In *Proceedings of the Twenty-Seventh International Conference on Machine Learning*, 399–406.
- Guo, Z.; Tang, Y.; Zhang, R.; Wang, D.; Wang, Z.; Zhao, B.; and Li, X. 2023. ViewRefer: Grasp the multi-view knowledge for 3D visual grounding. In *Proceedings of the IEEE International Conference on Computer Vision*, 15326–15337.
- Han, Z.; Yang, F.; Huang, J.; Zhang, C.; and Yao, J. 2022. Multimodal dynamics: Dynamical fusion for trustworthy multimodal classification. In *Proceedings of the IEEE Conference on Computer Vision and Pattern Recognition*, 20707–20717.
- Han, Z.; Zhang, C.; Fu, H.; and Zhou, J. T. 2021. Trusted multi-view classification. In *Proceedings of the Ninth International Conference on Learning Representations*, 1–11.
- Joukovsky, B.; Eldar, Y. C.; and Deligiannis, N. 2024. Interpretable neural networks for video separation: Deep unfolding RPCA with foreground masking. *IEEE Transactions on Image Processing*, 33: 108–122.
- Li, C.; Zhang, B.; Hong, D.; Yao, J.; and Chanussot, J. 2023. LRR-Net: An interpretable deep unfolding network for hyperspectral anomaly detection. *IEEE Transactions on Geoscience and Remote Sensing*, 61: 1–12.
- Lin, Y.; Gou, Y.; Liu, X.; Bai, J.; Lv, J.; and Peng, X. 2023. Dual contrastive prediction for incomplete multi-view representation learning. *IEEE Transactions on Pattern Analysis and Machine Intelligence*, 45(4): 4447–4461.
- Liu, J.; Hooi, B.; Kawaguchi, K.; and Xiao, X. 2022. MGNNI: Multiscale graph neural networks with implicit layers. In *Advances in Neural Information Processing Systems*, 21358–21370.
- Liu, J.; Kawaguchi, K.; Hooi, B.; Wang, Y.; and Xiao, X. 2021. EIGNN: Efficient infinite-depth graph neural networks. In *Advances in Neural Information Processing Systems*, 18762–18773.
- Liu, S.; Zhang, J.; Wen, Y.; Yang, X.; Wang, S.; Zhang, Y.; Zhu, E.; Tang, C.; Zhao, L.; and Liu, X. 2024. Sample-level cross-view similarity learning for incomplete multi-view clustering. In *Proceedings of the Thirty-Eighth AAAI Conference on Artificial Intelligence*, 14017–14025.
- Ning, X.; Yu, Z.; Li, L.; Li, W.; and Tiwari, P. 2024. DILF: Differentiable rendering-based multi-view image-language fusion for zero-shot 3D shape understanding. *Information Fusion*, 102: 102033.
- Pei, S.; Kou, Z.; Zhang, Q.; and Zhang, X. 2023. Few-shot low-resource knowledge graph completion with multi-view task representation generation. In *Proceedings of the Twenty-Ninth ACM SIGKDD Conference on Knowledge Discovery and Data Mining*, 1862–1871.
- Peng, X.; Li, Y.; Tsang, I. W.; Zhu, H.; Lv, J.; and Zhou, J. T. 2022. XAI beyond classification: Interpretable neural clustering. *Journal of Machine Learning Research*, 23: 1–28.

- Safaei, B.; VS, V.; de Melo, C. M.; and Patel, V. M. 2024. Entropic open-set active learning. In *Proceedings of the Thirty-Eighth AAAI Conference on Artificial Intelligence*, 4686–4694.
- Scheirer, W. J.; de Rezende Rocha, A.; Sapkota, A.; and Boulton, T. E. 2012. Toward open-set recognition. *IEEE Transactions on Pattern Analysis and Machine Intelligence*, 35(7): 1757–1772.
- Shukla, S.; Balasubramanian, S.; and Pavlović, M. 2016. A generalized Banach fixed point theorem. *Bulletin of the Malaysian Mathematical Sciences Society*, 39: 1529–1539.
- Song, S.; Zhao, S.; Wang, C.; Yan, T.; Li, S.; Mao, X.; and Wang, M. 2024. A dual-way enhanced framework from text matching point of view for multimodal entity linking. In *Proceedings of the Thirty-Eighth AAAI Conference on Artificial Intelligence*, 19008–19016.
- Tan, Y.; Cai, H.; Huang, S.; Wei, S.; Yang, F.; and Lv, J. 2024. An effective augmented Lagrangian method for fine-grained multi-view optimization. In *Proceedings of the Thirty-Eighth AAAI Conference on Artificial Intelligence*, 15258–15266.
- Wan, X.; Liu, X.; Liu, J.; Wang, S.; Wen, Y.; Liang, W.; Zhu, E.; Liu, Z.; and Zhou, L. 2023. Auto-weighted multi-view clustering for large-scale data. In *Proceedings of the Thirty-Seventh AAAI Conference on Artificial Intelligence*, 10078–10086.
- Wang, S.; Liu, X.; Liu, S.; Jin, J.; Tu, W.; Zhu, X.; and Zhu, E. 2022. Align then fusion: Generalized large-scale multi-view clustering with anchor matching correspondences. In *Advances in Neural Information Processing Systems*, 5882–5895.
- Wang, S.; Liu, X.; Liu, S.; Tu, W.; and Zhu, E. 2024. Scalable and structural multi-view graph clustering with adaptive anchor fusion. *IEEE Transactions on Image Processing*, 33: 4627–4639.
- Weerdt, B. D.; Eldar, Y. C.; and Deligiannis, N. 2024. Deep unfolding transformers for sparse recovery of video. *IEEE Transactions on Signal Processing*, 72: 1782–1796.
- Wu, Z.; Lin, X.; Lin, Z.; Chen, Z.; Bai, Y.; and Wang, S. 2023. Interpretable graph convolutional network for multi-view semi-supervised learning. *IEEE Transactions on Multimedia*, 25: 8593–8606.
- Wu, Z.; Xiao, M.; Fang, C.; and Lin, Z. 2024. Designing universally-approximating deep neural networks: A first-order optimization approach. *IEEE Transactions on Pattern Analysis and Machine Intelligence*, 46(9): 6231–6246.
- Xiao, S.; Du, S.; Chen, Z.; Zhang, Y.; and Wang, S. 2023. Dual fusion-propagation graph neural network for multi-view clustering. *IEEE Transactions on Multimedia*, 25: 9203–9215.
- Xiao, Y.; Zhang, J.; Liu, B.; Zhao, L.; Kong, X.; and Hao, Z. 2024. Multi-view maximum margin clustering with privileged information learning. *IEEE Transactions on Circuits and Systems for Video Technology*, 34(4): 2719–2733.
- Xu, C.; Si, J.; Guan, Z.; Zhao, W.; Wu, Y.; and Gao, X. 2024a. Reliable conflictive multi-view learning. In *Proceedings of the Thirty-Eighth AAAI Conference on Artificial Intelligence*, 16129–16137.
- Xu, G.; Wen, J.; Liu, C.; Hu, B.; Liu, Y.; Fei, L.; and Wang, W. 2024b. Deep variational incomplete multi-view clustering: Exploring shared clustering structures. In *Proceedings of the Thirty-Eighth AAAI Conference on Artificial Intelligence*, 16147–16155.
- Xu, J.; Chen, S.; Ren, Y.; Shi, X.; Shen, H.; Niu, G.; and Zhu, X. 2023. Self-weighted contrastive learning among multiple views for mitigating representation degeneration. In *Advances in Neural Information Processing Systems*, 1119–1131.
- Xu, J.; Li, W.; Liu, X.; Zhang, D.; Liu, J.; and Han, J. 2020. Deep embedded complementary and interactive information for multi-view classification. In *Proceedings of the Thirty-Fourth AAAI Conference on Artificial Intelligence*, 6494–6501.
- Yang, C.; Wen, H.; Hooi, B.; and Zhou, L. 2024. CapMax: A framework for dynamic network representation learning from the view of multiuser communication. *IEEE Transactions on Neural Networks and Learning Systems*, 35(4): 4554–4566.
- Yang, M.; Li, Y.; Hu, P.; Bai, J.; Lv, J. C.; and Peng, X. 2022. Robust multi-view clustering with incomplete information. *IEEE Transactions on Pattern Analysis and Machine Intelligence*, 45(1): 1055–1069.
- Yang, M.; Li, Y.; Huang, Z.; Liu, Z.; Hu, P.; and Peng, X. 2021. Partially view-aligned representation learning with noise-robust contrastive loss. In *Proceedings of the IEEE Conference on Computer Vision and Pattern Recognition*, 1134–1143.
- Ye, F.; and Li, S. 2024. MileCut: A multi-view truncation framework for legal case retrieval. In *Proceedings of the Thirty-Third ACM on Web Conference*, 1341–1349.
- Yu, S.; Wang, S.; Dong, Z.; Tu, W.; Liu, S.; Lv, Z.; Li, P.; Wang, M.; and Zhu, E. 2024a. A non-parametric graph clustering framework for multi-view data. In *Proceedings of the Thirty-Eighth AAAI Conference on Artificial Intelligence*, 16558–16567.
- Yu, S.; Wang, S.; Zhang, P.; Wang, M.; Wang, Z.; Liu, Z.; Fang, L.; Zhu, E.; and Liu, X. 2024b. DVSAI: Diverse view-shared anchors based incomplete multi-view clustering. In *Proceedings of the Thirty-Eighth AAAI Conference on Artificial Intelligence*, 16568–16577.
- Zhang, H.; Cissé, M.; Dauphin, Y. N.; and Lopez-Paz, D. 2018. Mixup: Beyond empirical risk minimization. In *Proceedings of the Sixth International Conference on Learning Representations*, 1–13.
- Zhang, P.; Wang, S.; Li, L.; Zhang, C.; Liu, X.; Zhu, E.; Liu, Z.; Zhou, L.; and Luo, L. 2023. Let the data choose: Flexible and diverse anchor graph fusion for scalable multi-view clustering. In *Proceedings of the Thirty-Seventh AAAI Conference on Artificial Intelligence*, 11262–11269.
- Zheng, Z.; Dai, W.; Xue, D.; Li, C.; Zou, J.; and Xiong, H. 2023. Hybrid ISTA: Unfolding ISTA with convergence

guarantees using free-form deep neural networks. *IEEE Transactions on Pattern Analysis and Machine Intelligence*, 45(3): 3226–3244.

Zhou, M.; Huang, J.; Zheng, N.; and Li, C. 2023. Learned image reasoning prior penetrates deep unfolding network for panchromatic and multi-spectral image fusion. In *Proceedings of the IEEE International Conference on Computer Vision*, 12364–12373.

Revisiting and Discussion

Algorithm 1: OpenViewer

Require: Multi-view original known data $\mathcal{D}_{original}$, training epochs T , batch iterations $B = \lceil \frac{N}{Batchsize} \rceil$, the number of unfolding layers L , **Beta** distribution parameter ω , trade-off parameters λ_1, λ_2 , distance margin ξ , and learning rate η .

Ensure: Obtain predictive distribution $P(\mathbf{Z}_{test})$.

- 1: Initialize network parameters $\Theta = \{\mathbf{R}, \mathbf{U}, \mathbf{M}, \theta_v, \rho_v\}$;
- 2: Initialize centroids $\{\mathbf{o}_v\}_{v=1}^V$ and center vectors $\{\mathbf{c}^{\mathcal{Y}_c}\}_{c=1}^C$;
- 3: **for** $t = 1 \rightarrow T$ **do**
- 4: **for** $b = 1 \rightarrow B$ **do**
- 5: Generate the pseudo-unknown data set $\mathcal{D}_{generated}$ by Eq. (1);
- 6: Concatenate $\mathcal{D}_{original}$ and $\mathcal{D}_{generated}$ to \mathcal{D}_{train} ;
- 7: **for** $l = 1 \rightarrow L$ **do**
- 8: Calculate and obtain the complementarity enhanced representation \mathbf{Z} by network (8);
- 9: **end for**
- 10: Compute the loss by open-set training regime (13);
- 11: Update Θ though backward propagation;
- 12: **end for**
- 13: **end for**
- 14: **return** Obtain predictive distribution $P(\mathbf{Z}_{test})$.

Revisiting. To address the openness challenges in multi-view learning within open environments, we propose a expression-enhanced deep unfolding network and a perception-augmented open-set training regime, designed to manage both known and unknown instances. OpenViewer decouples the multi-view integration process, enabling the model to effectively distinguish between known and unknown, thus mitigating issues of interpretability and generalization. OpenViewer promotes the expression of known and unknown through the unfolding network, ensuring that known parts are highly responsive while unknown parts highlight inappropriate confidences. Additionally, the loss assistance model further strengthens the confidences in known while suppressing undue confidences in unknown. OpenViewer can be summarized as Algorithm 1.

Discussion. 1) **Connections with Existing Multi-view Methods:** OpenViewer combines the prior knowledge and architecture of heuristic (Wang et al. 2022; Liu et al. 2024) and deep (Lin et al. 2023; Du et al. 2024) methods to adapt to unknown class samples while ensuring interpretability; 2) **Differences with Existing Interpretable and Open-set Methods:** Unlike existing interpretable methods (Wu et al. 2023; Weerd, Eldar, and Deligiannis 2024; Fang et al. 2024a), OpenViewer decouples model interpretability in mixed scenarios through multi-view priors, intuitively reflecting the essence and function of data operations during the integration process in openness multi-view learning. Furthermore, OpenViewer distinguishes itself from (Duan et al. 2023; Gou et al. 2024), as it is one of the few open-set approaches that simultaneously ensures the perception of both

known and unknown instances in multi-view scenarios while also addressing interpretability.

Supplementary of Interpretability Boundary

Certainly, the construction of network modules in OpenViewer adheres to the characteristics commonly associated with heuristic methods. As a result, by employing the conventional approach of heuristic methods and updating each sub-variable problem using ADMM, we can theoretically ensure the interpretability boundary of OpenViewer. Moreover, if we establish the interpretability boundary of each individual module, it naturally follows that OpenViewer, comprising these modules, will also converge and be bounded. Embracing these principles will guide us in proving and analyzing the interpretability boundary of OpenViewer. For the convenience of analysis, we can divide these modules into two classes: RF-Module, CD-Module, and DN-Module with parameter updating, and CW-Fusion modules only need self-optimization without parameters. Then, the boundary will also be analyzed according to this classification. If they are all convergent, then as the previous analysis, their overall combination can also ensure boundness.

CW-Fusion: In theory, this module converges due to the stability of weight calculation and the characteristics of linear combination.

RF-Module, CD-Module, and DN-Module: Unlike the above modules, these are iterative network modules with parameters and cannot be subjected to analyze as the above modules. Fortunately, several works (Liu et al. 2021, 2022) have provided us with ideas for analyzing the boundness of such modules. Following them, we first need to introduce **Definition 1** of the Banach fixed Point Theorem (Shukla, Balasubramanian, and Pavlović 2016) as a preparation.

Definition 1. Let (\mathbf{X}, d) be a non-empty complete metric space with a contraction mapping $T : \mathbf{X} \rightarrow \mathbf{X}$. If there exists a $\mu \in [0, 1)$ that makes $d(T(\mathbf{x}), T(\mathbf{y})) \leq \mu d(\mathbf{x}, \mathbf{y}), \forall \mathbf{x}, \mathbf{y} \in \mathbf{X}$. Then, a contraction T admits a unique fixed-point \mathbf{x}^* in \mathbf{X} (i.e., $T(\mathbf{x}^*) = \mathbf{x}^*$). Furthermore, \mathbf{x}^* can be found as follows: Start with an arbitrary element $\mathbf{x}_0 \in \mathbf{X}$ and define a sequence $\{\mathbf{x}_n\}_{n \in \mathbb{N}}$ by $\mathbf{x}_n = T\{\mathbf{x}_{n-1}\}$ for $n \geq 1$. Then $\lim_{n \rightarrow \infty} \mathbf{x}_n = \mathbf{x}^*$.

With the help of **Definition 1**, we can transit to **Theorem 3**.

Theorem 3. Given the bounded damping factor $\mu \in [0, 1)$, the modules for propagation is a contraction mapping, and the unique convergence solution \mathbf{X}^* can be obtained.

Proof. For any matrix $\mathbf{B} \in \mathbb{R}^{B_1 \times B_2}$, we define the vectorization of the matrix by $vec[\mathbf{B}] \in \mathbb{R}^{B_1 \times B_2}$ and the Frobenius norm of the matrix by $\|\mathbf{B}\|_F$. Let us first state some preliminary explanation for the framework derived networks in Table 1. On this premise, we define the mapping function φ that contains the proximal operator $\mathcal{S}_{\theta_v^{(t)}}$. Then, $\varphi(\mathbf{Z}_v) = \mathbf{Z}_v \mathbf{R} + (\mathbf{X}_v - \mathbf{E}_v) \mathbf{D}_v^\top \mathbf{U}$, and we want to present that the map φ is contraction. Using the property of the vectorization

| Variant Models | Concretized Optimization Problems | Composition of Deep Unfolding Network Modules |
|----------------|---|---|
| OpenSViewer | $\min_{\mathbf{Z}_v} \sum_{v=1}^V (\frac{1}{2} \ \mathbf{X}_v - \mathbf{Z}_v \mathbf{D}_v\ _F^2 + \alpha \ \mathbf{Z}_v\ _1)$ | RF-Module: $\mathbf{Z}_v^{(l+1)} \leftarrow \mathcal{S}_{\theta_v^{(l)}}(\mathbf{Z}_v^{(l)} \mathbf{R} + \mathbf{X}_v \mathbf{U})$ CW-Fusion: $\mathbf{Z}^{(l+1)} \leftarrow \sum_{v=1}^V \mathbf{w}_v^{(l+1)} \mathbf{Z}_v^{(l+1)}$ |
| OpenSDViewer | $\min_{\mathbf{Z}_v, \mathbf{D}_v} \sum_{v=1}^V (\frac{1}{2} \ \mathbf{X}_v - \mathbf{Z}_v \mathbf{D}_v\ _F^2 + \alpha \ \mathbf{Z}_v\ _1 + \frac{\beta}{2} \ \mathbf{D}_v\ _F^2)$ | RF-Module: $\mathbf{Z}_v^{(l+1)} \leftarrow \mathcal{S}_{\theta_v^{(l)}}(\mathbf{Z}_v^{(l)} \mathbf{R} + \mathbf{X}_v (\mathbf{D}_v^\top)^{(l)} \mathbf{U})$ CD-Module: $\mathbf{D}_v^{(l+1)} \leftarrow \mathbf{M}(\mathbf{Z}_v^\top)^{(l+1)} \mathbf{X}_v$ CW-Fusion: $\mathbf{Z}^{(l+1)} \leftarrow \sum_{v=1}^V \mathbf{w}_v^{(l+1)} \mathbf{Z}_v^{(l+1)}$ |
| OpenViewer | $\min_{\mathbf{Z}_v, \mathbf{D}_v, \mathbf{E}_v} \sum_{v=1}^V (\frac{1}{2} \ \mathbf{X}_v - \mathbf{Z}_v \mathbf{D}_v - \mathbf{E}_v\ _F^2 + \alpha \ \mathbf{Z}_v\ _1 + \frac{\beta}{2} \ \mathbf{D}_v\ _F^2 + \gamma \ \mathbf{E}_v\ _{2,1})$ | RF-Module: $\mathbf{Z}_v^{(l+1)} \leftarrow \mathcal{S}_{\theta_v^{(l)}}(\mathbf{Z}_v^{(l)} \mathbf{R} + (\mathbf{X}_v - \mathbf{E}_v^{(l)}) (\mathbf{D}_v^\top)^{(l)} \mathbf{U})$ CD-Module: $\mathbf{D}_v^{(l+1)} \leftarrow \mathbf{M}(\mathbf{Z}_v^\top)^{(l+1)} (\mathbf{X}_v - \mathbf{E}_v^{(l)})$ DN-Module: $\mathbf{E}_v^{(l+1)} \leftarrow \mathcal{P}_{\rho_v^{(l)}}(\mathbf{X}_v - \mathbf{Z}_v^{(l+1)} \mathbf{D}_v^{(l+1)})$ CW-Fusion: $\mathbf{Z}^{(l+1)} \leftarrow \sum_{v=1}^V \mathbf{w}_v^{(l+1)} \mathbf{Z}_v^{(l+1)}$ |

Table 1: The generalized objective problem (2) leverages the ADMM optimizer to obtain the deep unfolding network (8). This inspires various multi-view ablation deep unfolding networks with diverse modules combination.

vec and the Kronecker product \otimes ,

$$\begin{aligned}
vec[\varphi(\mathbf{Z}_v)] &= vec[\mathbf{Z}_v \mathbf{R}] + vec[(\mathbf{X}_v - \mathbf{E}_v) \mathbf{D}_v^\top \mathbf{U}] \\
&= [(\mathbf{R})^\top] vec[\mathbf{Z}_v] + vec[(\mathbf{X}_v - \mathbf{E}_v) \mathbf{D}_v^\top \mathbf{U}] \\
&= \mu \left([(\mathbf{F})^\top \otimes \mathbf{A}] vec[\mathbf{Z}_v] + vec[(\mathbf{X}_v - \mathbf{E}_v) \mathbf{D}_v^\top \mathbf{U}] \right),
\end{aligned} \tag{14}$$

where μ is an extracted parameter, and $\mathbf{A} \in \mathbb{R}^{N \times N}$ is a matrix whose diagonal element is $\frac{1}{\mu}$ and the rest is 0. Therefore, for any $\mathbf{Z}_v, \mathbf{Z}'_v \in \mathbb{R}^{N \times C}$,

$$\begin{aligned}
\|\varphi(\mathbf{Z}_v) - \varphi(\mathbf{Z}'_v)\|_F &= \|vec[\varphi(\mathbf{Z}_v)] - vec[\varphi(\mathbf{Z}'_v)]\|_2 \\
&= \left\| \mu \left([(\mathbf{F})^\top \otimes \mathbf{A}] (vec[\mathbf{Z}_v] - vec[\mathbf{Z}'_v]) \right) \right\|_2 \\
&\leq \mu \left\| [(\mathbf{F})^\top \otimes \mathbf{A}] \right\|_2 \|vec[\mathbf{Z}_v] - vec[\mathbf{Z}'_v]\|_2.
\end{aligned} \tag{15}$$

Due to all matrices and layers are normalized, which means the spectral radius of $A = [(\mathbf{F})^\top \otimes \mathbf{A}] \in [0, \frac{1}{\mu} - \frac{1}{\mu L_{p_v}}]$, and the range of $\|A\|_2$ belongs to $[0, 1)$,

$$\|\varphi(\mathbf{Z}_v) - \varphi(\mathbf{Z}'_v)\|_F \leq \underbrace{\mu \left\| [(\mathbf{F})^\top \otimes \mathbf{A}] \right\|_2}_{[0,1)} \tag{16}$$

$$\|vec[\mathbf{Z}_v] - vec[\mathbf{Z}'_v]\|_2 \leq \mu \|\mathbf{Z}_v - \mathbf{Z}'_v\|_F.$$

Since $\mu \in [0, 1)$, this illustrates that φ is a contraction mapping on the metric space $(\mathbb{R}^{N \times C}, \hat{d})$, where $\hat{d}(\mathbf{Z}_v, \mathbf{Z}'_v) = \|\mathbf{Z}_v - \mathbf{Z}'_v\|_F$. Therefore, this module has a convergence lower bound, and the proof is completed. \square

Similarly, we can also prove the boundness of other modules as above. By leveraging the properties of matrix vectorization, the Kronecker product, and **Definition 1**, the boundness of these interpretable modules can be demonstrated by **Theorem 3**. By ensuring the boundness of each of the four modules, we can establish the following **Theorem 4**.

Theorem 4. (Interpretability Boundary) *If each sub-module is convergent, then the stacked deep unfolding network consisting of all modules is bounded.*

Proof. Since each sub-module gradually approaches its own optimal value, their joint deep unfolding network obtain the bounded solution of a large global problem by coordinating the sub-module solutions until convergence. \square

Theorem 4 ensures that the deep network exported through the ADMM method will be bounded to the same solution regardless of which starting point the iteration starts from. This indicates that even in the face of different views, through interpretable operations, it is possible to ensure that information from these different views can be reasonably integrated, thereby improving the trustworthiness of feature expression enhancement. It also ensures that the network has interpretable theoretical guarantees.

At this point, we have ensured the interpretability boundness of unfolding networks through **Theorem 4**.

Supplementary of Generalization Support

Here, (Peng et al. 2022) provides us with some ideas to prove the overall convergence. First, we use the standard gradient descent methods to update parameters Θ as $\Theta_{t+1} = \Theta_t - \eta_t \nabla \mathcal{L}_{total}(\Theta_t)$, where η_t is a learning rate, $\nabla \mathcal{L}_{total}$ denotes the gradient of total losses, and we need to introduce **Definition 2** as follows.

Definition 2. *A function $f(x)$ is Lipschitz continuous on the set Φ , if there exists a constant $\epsilon > 0$, $\forall x_1, x_2 \in \Phi$ such that $\|f(x_1) - f(x_2)\| \leq \epsilon \|x_1 - x_2\|$, where ϵ is the Lipschitz constant.*

Namely, the objective function $\mathcal{L}_{total}(\Theta)$ is Lipschitz continuous *i.i.f.* $\|\mathcal{L}_{total}\| \leq \epsilon$. In other words, to meet the Lipschitz continuity, we need to prove that the upper boundary of $\nabla \mathcal{L}_{total}$ exists. To this end, we propose **Theorem 5**.

Theorem 5. *There exist $\epsilon > 0$ such as $\nabla \mathcal{L}_{total} \leq \epsilon$, where ϵ can be $\frac{1}{N\sigma} \|\hat{\mathbf{p}}_c^{(i)}\| + \frac{1}{N\sigma} \|\hat{\mathbf{y}}_c^{(i)}\| + 2 \|\hat{\mathbf{z}}^{(i)}\| + 2\xi + \lambda_1(\frac{1}{C} \|\tilde{\mathbf{p}}^{(i)}\| + \frac{1}{C} + 2 \|\tilde{\mathbf{z}}^{(i)}\|) + \lambda_2(\|\hat{\mathbf{z}}_c^{(i)}\| + \|\mathbf{c}^{\hat{\mathbf{y}}_c^{(i)}}\| + \varphi)$ at least.*

Proof. The derivation of \mathcal{L}_{known} , $\mathcal{L}_{unknown}$, and \mathcal{L}_{center} are performed separately as

$$\nabla \mathcal{L}_{known}(\hat{\mathbf{z}}^{(i)}) = \frac{1}{N^o} \left(\hat{\mathbf{p}}_c^{(i)} - \hat{\mathbf{y}}_c^{(i)} \right) + 2(\|\hat{\mathbf{z}}^{(i)}\| - \xi) \cdot \frac{\hat{\mathbf{z}}^{(i)}}{\|\hat{\mathbf{z}}^{(i)}\|}, \quad (17)$$

$$\nabla \mathcal{L}_{unknown}(\tilde{\mathbf{z}}^{(i)}) = \frac{1}{C} \left(\tilde{\mathbf{p}}^{(i)} - 1 \right) + 2\tilde{\mathbf{z}}^{(i)}, \quad (18)$$

$$\nabla \mathcal{L}_{center}(\hat{\mathbf{z}}_c^{(i)}) = \left(\hat{\mathbf{z}}_c^{(i)} - \mathbf{c}^{\hat{\mathbf{y}}_c^{(i)}} \right) + \lambda \frac{\delta(\hat{\mathbf{y}}_c^{(i)} = j)}{1 + \sum_{i=1}^{N^o} \delta(\hat{\mathbf{y}}_c^{(i)} = j)}, \quad (19)$$

where $\hat{\mathbf{p}}_c^{(i)} = P(\hat{\mathbf{z}}^{(i)}) = \frac{e^{\hat{\mathbf{z}}^{(i)}}}{\sum_{j=1}^C e^{\hat{\mathbf{z}}_j^{(i)}}$, $\tilde{\mathbf{p}}^{(i)} = P(\tilde{\mathbf{z}}^{(i)})$. Then,

according to the properties of matrices and their inequalities, the following inequalities hold,

$$\|\nabla \mathcal{L}_{known}(\hat{\mathbf{z}}^{(i)})\| \leq \frac{1}{N^o} (\|\hat{\mathbf{p}}_c^{(i)}\| + \|\hat{\mathbf{y}}_c^{(i)}\|) + 2(\|\hat{\mathbf{z}}^{(i)}\| + \xi), \quad (20)$$

$$\|\nabla \mathcal{L}_{unknown}(\tilde{\mathbf{z}}^{(i)})\| \leq \frac{1}{C} (\|\tilde{\mathbf{p}}^{(i)}\| + 1) + 2\|\tilde{\mathbf{z}}^{(i)}\|, \quad (21)$$

$$\|\nabla \mathcal{L}_{center}(\hat{\mathbf{z}}_c^{(i)})\| \leq \|\hat{\mathbf{z}}_c^{(i)}\| + \|\mathbf{c}^{\hat{\mathbf{y}}_c^{(i)}}\| + \varphi, \quad (22)$$

where $\varphi = \lambda \frac{\delta(\hat{\mathbf{y}}_c^{(i)} = j)}{1 + \sum_{i=1}^{N^o} \delta(\hat{\mathbf{y}}_c^{(i)} = j)}$, λ is a constant, $0 \leq \|\hat{\mathbf{p}}\| \leq 1$, $0 \leq \|\tilde{\mathbf{p}}\| \leq 1$, $0 \leq \|\hat{\mathbf{z}}\| \leq 1$, and $0 \leq \|\tilde{\mathbf{z}}\| \leq 1$. Finally, based on all the above statements, we can obtain the following boundary inequalities as

$$\|\nabla \mathcal{L}_{total}(\mathbf{z})\| \leq \|\nabla \mathcal{L}_{known}(\hat{\mathbf{z}})\| + \lambda_1 \|\nabla \mathcal{L}_{unknown}(\tilde{\mathbf{z}})\| + \lambda_2 \|\nabla \mathcal{L}_{center}(\hat{\mathbf{z}})\|, \quad (23)$$

where $\mathbf{z} = \{\hat{\mathbf{z}}, \tilde{\mathbf{z}}\}$. It showcases that the training loss function $\mathcal{L}_{total}(\Theta)$ will be upper bounded by a positive real number ϵ when $\|\mathbf{z}\|$ is bounded. At this point, the proof is completed. In fact, there exists the upper boundary of $\|\mathbf{z}\|$ for any real-world datasets. \square

Based on **Theorem 5**, we have the following convergence **Theorem 6**. $\mathcal{L}_{total}(\Theta)$ is abbreviated as \mathcal{L} .

Theorem 6. *One could always find an optimal loss $\mathcal{L}_T^*(\Theta)$, which is sufficiently close to the desired $\mathcal{L}^*(\Theta)$ after T*

$$\text{epochs, i.e., } \mathcal{L}_T^* - \mathcal{L}^* \leq \frac{\|\Theta_1 - \Theta^*\|_F^2 + \epsilon^2 \sum_{t=1}^T (\eta_t)^2}{2 \sum_{t=1}^T \eta_t}.$$

Proof. Let Θ^* be the optimal parameters of OpenViewer, Θ_T be the T -th parameters, and then we have

$$\|\Theta_{T+1} - \Theta^*\|_F^2 = \|\Theta_T - \Theta^*\|_F^2 - 2 \text{tr}(\eta_T \nabla \mathcal{L}_T^\top (\Theta_T - \Theta^*)) + \eta_T^2 \|\nabla \mathcal{L}_T\|_F^2. \quad (24)$$

By recursively applying the above equation, we obtain

$$\|\Theta_{T+1} - \Theta^*\|_F^2 = \|\Theta_1 - \Theta^*\|_F^2 - 2 \sum_{t=1}^T \eta_t \text{tr}(\Theta_t - \Theta^*) + \sum_{t=1}^T \eta_t^2 \|\nabla \mathcal{L}_t\|_F^2. \quad (25)$$

As $\mathcal{L}(\cdot)$ satisfies the Lipschitz Continuity and according to the definition of gradient, i.e.,

$$f(x^*) \geq f(x_t) + \nabla \mathcal{L}_t^\top (x^* - x_t), \quad (26)$$

and then, we have

$$\|\Theta_{T+1} - \Theta^*\|_F^2 \leq \|\Theta_1 - \Theta^*\|_F^2 - 2 \sum_{t=1}^T \eta_t (\mathcal{L}_t - \mathcal{L}^*) + \epsilon^2 \sum_{t=1}^T \eta_t^2, \quad (27)$$

$$2 \sum_{t=1}^T \eta_t (\mathcal{L}_t - \mathcal{L}^*) \leq \|\Theta_1 - \Theta^*\|_F^2 + \epsilon^2 \sum_{t=1}^T \eta_t^2, \quad (28)$$

$$\mathcal{L}_T - \mathcal{L}^* \geq \min_{t=1,2,\dots,T} (\mathcal{L}_t - \mathcal{L}^*) = \mathcal{L}_T^* - \mathcal{L}^*, \quad (29)$$

where \mathcal{L}_T^* is the best \mathcal{L} found in T epochs. Combining inequalities (28)-(29), we finally have

$$\mathcal{L}_T^* - \mathcal{L}^* \leq \frac{\|\Theta_1 - \Theta^*\|_F^2 + \epsilon^2 \sum_{t=1}^T \eta_t^2}{2 \sum_{t=1}^T \eta_t}. \quad (30)$$

Here, the proof is completed. \square

Grounded on **Theorem 6**, we could derive **Theorem 7**.

Theorem 7. (Generalization Support) *For the fixed step size (i.e., $\eta_t = \eta$) as $T \rightarrow \infty$, and given the existing upper bound of positive real number ϵ , the difference $\mathcal{L}_T^* - \mathcal{L}^*$ generalizes to $\frac{\eta\epsilon^2}{2}$ with a convergence rate $\mathcal{O}(\frac{1}{T})$.*

Proof. After T epochs, we have

$$\begin{aligned} \mathcal{L}_T^* - \mathcal{L}^* &\leq \frac{\|\Theta_1 - \Theta^*\|_F^2 + T\epsilon^2\eta^2}{2T\eta} \\ &= \frac{\|\Theta_1 - \Theta^*\|_F^2 / (T\eta) + \eta\epsilon^2}{2}. \end{aligned} \quad (31)$$

The first term decreases at the rate of $\frac{1}{T}$, while the second term is a constant term for a fixed learning rate η . Therefore, the convergence rate of the proposed method is $\mathcal{O}(\frac{1}{T})$ and the convergence radius is $\frac{\eta\epsilon^2}{2}$ with the upper bound of positive real number ϵ . Here, the proof is completed. \square

Theorem 7 highlights that will ultimately converge to \mathcal{L}^* , exhibiting a convergence radius of $\frac{\eta\epsilon^2}{2}$ within T epochs. Generalization support ensures that the OpenViewer's training loss continually approaches its optimum with increased iterations, which is crucial for handling multi-view data in open environments: 1) It demonstrates the OpenViewer's long-term generalization and stability, ensuring that even with complex data and open environments, OpenViewer can theoretically approach the optimal solution after sufficient iterations; 2) It ensures that the integration of information from different views converges to a consistent solution, reducing noise and improving the accuracy of overall decisions or predictions; 3) In open environments, when encountering unknown classes or data, OpenViewer can maintain stable generalization through appropriate adjustments; 4) It reinforces the theoretical foundation of other OpenViewer-like algorithm design, ensuring its reliability and effectiveness in practical open-setting applications.

Theoretical Analysis: Complexity

Then, we analyze the complexity of OpenViewer in each batch, including network modules and losses of the time and space complexity.

The time complexity of the proposed network modules is summarized as follows: **RF-Module**: The primary operations involve matrix multiplications with complexities $\mathcal{O}(NC^2)$ and $\mathcal{O}(NCD_v)$, resulting in an overall complexity of $\mathcal{O}(NC^2 + NCD_v)$. **CD-Module**: It includes operations such as $\mathbf{Z}_v^\top (\mathbf{X}_v - \mathbf{E}_v^{(l)})$. Thus, the total complexity is $\mathcal{O}(NCD_v)$. **DN-Module**: The key computations are $\mathbf{Z}_v^{(l+1)} \mathbf{D}_v^{(l+1)}$ and subtraction $(\mathbf{X}_v - \mathbf{Z}_v^{(l+1)} \mathbf{D}_v^{(l+1)})$, with a combined complexity of $\mathcal{O}(NCD_v)$. **CW-Fusion**: The fusion process is dominated by the centroid computation $\mathcal{O}(NCD_v)$, inter-class distance calculation $\mathcal{O}(C^2D_v)$, and the weighted fusion operation $\mathcal{O}(NCV)$, resulting in a complexity of $\mathcal{O}(NCD_v + C^2D_v + NCV)$. Combining these, the total time complexity for the deep networks is $\mathcal{O}(NC(C + D_v + V) + C^2D_v)$. Moreover, the space complexity of the deep unfolding networks is $\mathcal{O}(N(D_v + C)V)$ with the storage requirements for feature matrices, dictionaries, and fusion weights.

The time complexity of training loss components is shown as follows: 1) \mathcal{L}_{known} has a time complexity of $\mathcal{O}(N^oC)$, due to the cross-entropy calculation and margin distance term; 2) The time complexity of $\mathcal{L}_{unknown}$ is $\mathcal{O}(N^eC + N^eD_v)$, due to both the cross-entropy loss and regularization term; 3) \mathcal{L}_{center} has a time complexity of $\mathcal{O}(N^oC + N^o)$ for computing the distance between samples and their class centers and updating the class centers. In summary, the overall time complexity for the loss functions is $\mathcal{O}(N^oC + N^eD_v)$. Furthermore, the space complexity of the training losses is $\mathcal{O}(NC + ND_v)$, encompassing the storage for predictions, centers, and intermediate calculations.

Overall, the time complexity of OpenViewer with L layers costs $\mathcal{O}((NC(C + D_v + V) + C^2D_v)L)$, and the space complexity of OpenViewer denotes $\mathcal{O}(N(D_v + C)V)$.

Supplementary of Experiments

In this section, we present supplementary of experiments, including datasets, compared methods, and other results.

Details of Datasets and Compared Methods

Datasets. Details for all test multi-view datasets are presented below. Multi-feature datasets: 1) **Animals**¹ is a deep multi-feature dataset that consists of 10,158 images from 50 animal classes with DECAF and VGG-19 features; 2) **AWA**² is a large-scale dataset belonging to 50 animal categories, we extract of 6 features for all the images, that is, color histogram, local self-similarity, pyramidHOG, SIFT, colorSIFT, and SURF features; 3) **NUSWIDE OBJ**³ consists of 30,000 images distributed over 31 classes. We use five

¹<http://attributes.kyb.tuebingen.mpg.de/>

²<https://cvml.ista.ac.at/AwA/>

³<https://lms.comp.nus.edu.sg/research/NUS-WIDE.htm>

features provided by NUS, *i.e.*, color histogram, color moments, color correlation, edge distribution and wavelet texture features; 4) **VGGFace2-50**⁴ is a large-scale face recognition dataset. We extract a sub-dataset with 50 face categories, which consists of four features as LBP, HOG, GIST, Gabor features. Multi-modal datasets: 1) **ESP-Game**⁵ originates from an image annotation game played on a website, which contains 20,770 images, and each image is annotated by players with several descriptions. Among them, image features are extracted by VGG-19 networks, and text description features are extracted by BERT networks. Here, we choose 11,032 images that are described with approximately five tags per image, and these images have a total of 7 classes; 2) **NUSWIDE20k**⁶ is real-world web image database sourced from Flickr, which consists of 269,648 social images with tags. Meanwhile, we select a sub-dataset with 20,000 images, which contains 8 classes and each image is along with seven tags on average.

Compared Methods. These comparison methods are described as follows. 1) **MvNNcor** (Xu et al. 2020) modeled view-specific information and cross-correlations information through an interactive network to jointly make decisions and infer categories; 2) **TMC** (Han et al. 2021) fused the uncertainty of multiple views at an evidence level with the Dempster-Shafer theory; 3) **MMDynamics** (Han et al. 2022) introduced a trustworthy approach to multi-modal classification by dynamically evaluating feature-level and modality-level informativeness; 4) **IMvGCN** (Wu et al. 2023) enhanced the interpretability of neural networks by constructing a flexible graph filter and introducing orthogonal normalization; 5) **LGCN-FF** (Chen et al. 2023) integrated sparse autoencoders with a learnable GCN, enabling the simultaneous extraction of feature representations and node relationships within graphs; 6) **ORLNet** (Fang et al. 2024a) derived an interpretable solution for explicit optimization representation learning objectives; 7) **RCML** (Xu et al. 2024a) provided decision results and attached reliabilities for conflictive multi-view data. These multi-view models are trained and tested according to their own structure and utilize the same dataset settings as OpenViewer to test their performance in an open environment.

Supplementary of Experimental Results

Fig. 1 supplements the t-SNE visualization results of all compared and ablation methods’s representations \mathbf{Z} on ESP-Game dataset. Fig. 2 presents the heatmap visualization results of the correlation matrices \mathbf{ZZ}^T for all compared methods on the Animals dataset. In OpenViewer’s heatmap, the known parts exhibit clearly enhanced expression, while the unknown parts are effectively suppressed, preventing excessive responses to the known parts. In contrast, other methods like MvNNCor, MMDynamics, LGCN-FF, and ORLNet reveal noise and overconfidence between the known and unknown categories. The enhanced expression effect of

⁴https://www.robots.ox.ac.uk/~vgg/data/vgg_face2/

⁵<https://www.kaggle.com/datasets/parhamsalar/espgame>

⁶<https://lms.comp.nus.edu.sg/wp-content/uploads/2019/research/nuswide/NUS-WIDE.html>

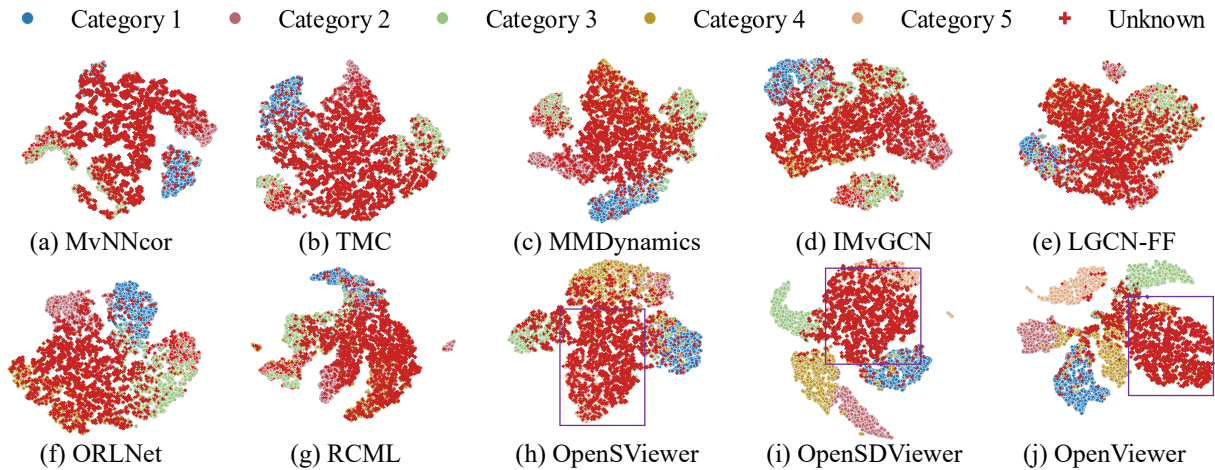


Figure 1: All compared methods' t-SNE visualizations based on the representations \mathbf{Z} of ESP-Game dataset.

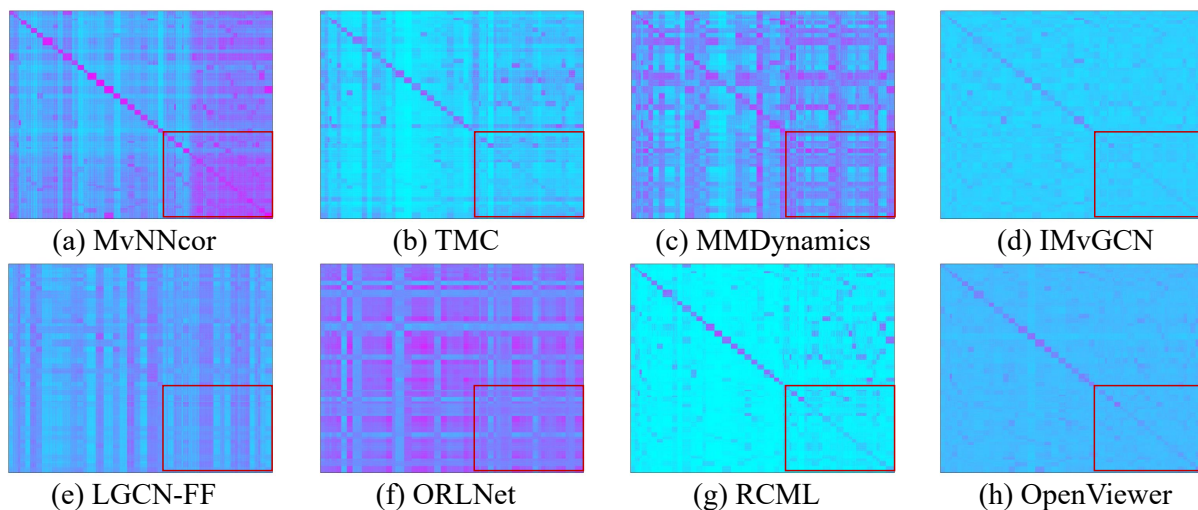


Figure 2: All compared methods' heatmap visualizations based on $\mathbf{Z}\mathbf{Z}^T$ of Animals dataset.

IMvGCN is less significant across all parts. Among the comparison methods, RCML performs the best, but there are still some outliers that affect recognition.

Supplementary of Parameter Sensitivity Analysis

Fig. 3 indicates the optimal number of unfolding layers for OpenViewer. The figure displays that with a single unfolding layer, the model effectively balances complexity and efficiency while maintaining interpretable expression-enhancement capabilities. Although performance may improve slightly on certain datasets with additional layers, the complexity also increases correspondingly. For this reason, we set the number of unfolding layers to $L = 1$ in our experiment. Fig. 4 provides all sensitivity curves for two trade-off parameters of training losses of OpenViewer, λ_1 and λ_2 . Fig. 5 showcases the representations \mathbf{Z} through the heatmaps of $\mathbf{Z}\mathbf{Z}^T$ across progressive training epochs. The figure clearly displays that, initially, \mathbf{Z} is saturated with noise and exhibits

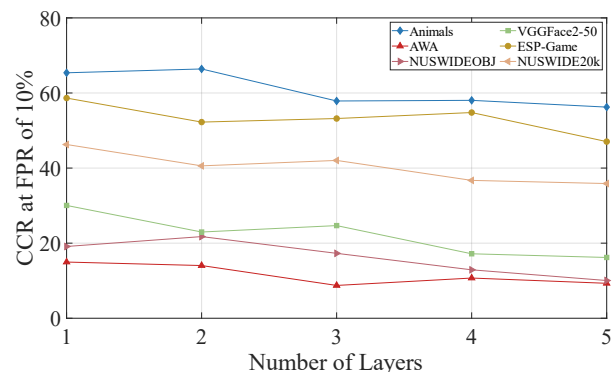


Figure 3: Parameter sensitivity of unfolding layers.

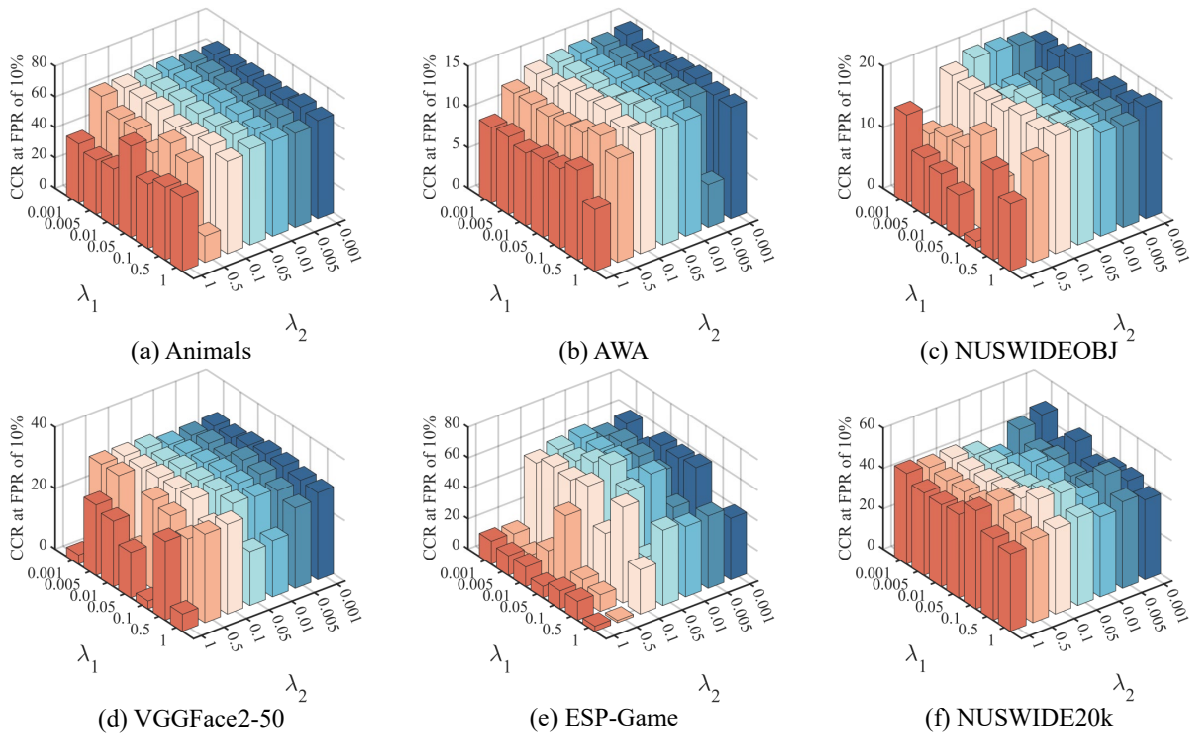


Figure 4: Parameter sensitivity of λ_1 and λ_2 of OpenViewer.

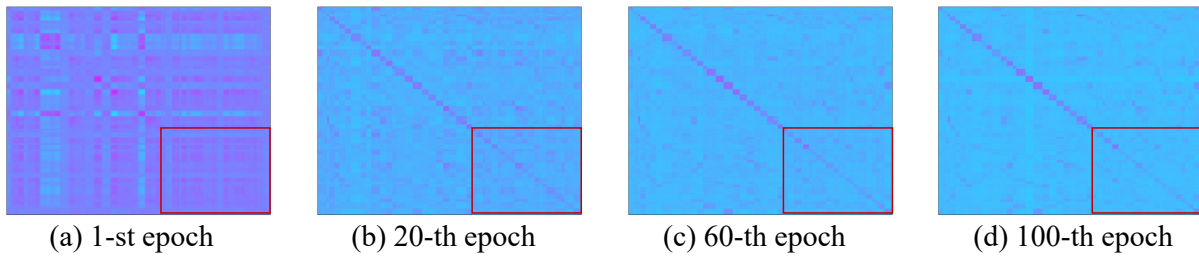


Figure 5: The heatmaps \mathbf{ZZ}^T as the changes over epochs of Animals dataset.

weak expression. As training epochs progress, noise is gradually eliminated, leading to an enhanced representation of known samples. Subsequently, the confidence of unknown samples on known classes (highlighted within the red box) are progressively suppressed. This progression substantiates OpenViewer’s contributions to enhanced feature expression and augmented sample perception.